EXPERIMENTAL INVESTIGATION OF THE EFFECT OF TEMPERATURE ON FRICTION PRESSURE LOSS OF POLYMERIC DRILLING FLUID THROUGH VERTICAL CONCENTRIC ANNULUS

A THESIS SUBMITTED TO
THE GRADUATE SCHOOL OF NATURAL AND APPLIED SCIENCES
OF
MIDDLE EAST TECHNICAL UNIVERSITY

BY

KAZIM ONUR GÜRÇAY

IN PARTIAL FULFILLMENT OF THE REQUIREMENTS
FOR
THE DEGREE OF MASTER OF SCIENCE
IN
PETROLEUM AND NATURAL GAS ENGINEERING

SEPTEMBER, 2018

Approval of the Thesis:

EXPERIMENTAL INVESTIGATION OF THE EFFECT OF TEMPERATURE ON FRICTION PRESSURE LOSS OF POLYMERIC DRILLING FLUID THROUGH VERTICAL CONCENTRIC ANNULUS

submitted by **KAZIM ONUR GÜRÇAY** in partial fulfillment of the requirements for the degree of **Master of Science in Petroleum and Natural Gas Engineering Department, Middle East Technical University** by,

Prof. Dr. Halil Kalıpçılar
Dean, Graduate School of **Natural and Applied Sciences** ________________

Prof. Dr. Serhat Akın
Head of Department, **Petroleum and Natural Gas Engineering** ________________

Prof. Dr. Serhat Akın
Supervisor, **Petroleum and Natural Gas Engineering Dept., METU** ________________

Assoc. Prof. Dr. İsmail Hakkı Gücüyener
Co Supervisor, **GEOS Energy Inc.** ________________

Examining Committee Members:

Assoc. Prof. Dr. Çağlar Sınayuç
Petroleum and Natural Gas Engineering Dept., METU ________________

Prof. Dr. Serhat Akın
Petroleum and Natural Gas Engineering Dept., METU ________________

Asst. Prof. Dr. Tuna Eren
Petroleum and Natural Gas Engineering Dept., ________________
Izmir Katip Celebi University

Date: 07.09.2018

I hereby declare that all information in this document has been obtained and presented in accordance with academic rules and ethical conduct. I also declare that, as required by these rules and conduct, I have fully cited and referenced all material and results that are not original to this work.

Name, Last name: Kazım Onur Gürçay

Signature:

ABSTRACT

EXPERIMENTAL INVESTIGATION OF THE EFFECT OF TEMPERATURE ON FRICTION PRESSURE LOSS OF POLYMERIC DRILLING FLUID THROUGH VERTICAL CONCENTRIC ANNULUS

Gürçay, Kazım Onur

M.S., Department of Petroleum and Natural Gas Engineering

Supervisor: Prof. Dr. Serhat Akın

Co-Supervisor: Assoc. Prof. Dr. İsmail Hakkı Gücüyener

September 2018, 88 pages

Accurate estimation of friction pressure loss through annulus is important to avoid lost circulation, pipe sticking, kicks or more serious problems in drilling and well completion operations. Several studies have been performed to determine friction pressure loss experimentally and theoretically through pipe and annulus with the effects of eccentricity, pipe rotation, annulus geometry or flow regime by applying several rheological models. However, in addition to all of these factors, fluid rheology is dependent on temperature. Change in rheological properties of fluid also leads to shift in friction pressure loss. However, experimental studies about the effect of temperature on friction pressure loss for the flow of non-Newtonian fluids have not been conducted.

This study experimentally investigated the effect of temperature on friction pressure loss through vertical concentric annulus (2.91 in X 1.85 in) with a polymerized drilling fluid including Polyanionic Cellulose (0.50 lb/bbl) and Xanthan Gum (0.75 lb/bbl). Friction pressure loss was determined with Herschel-Bulkley rheological model which has less error than Bingham Plastic and Power Law rheological models by comparing measured and calculated shear stresses with four different equivalent diameter concepts. Also, the most suitable equivalent diameter concept was chosen as hydraulic radius in laminar

region, slot approximation in turbulent region by comparing experimental and theoretical results of friction pressure loss and flow rate.

Temperature effects on rheological parameters, Reynolds number and apparent viscosity were investigated. Among rheological parameters, consistency index (K) and yield point (YP) were more sensitive to the effect of temperature than flow behavior index (n). Reynolds number and apparent viscosity vs. temperature plots with flow rates changing from 25 to 125 gpm were examined and it was observed that high shear rate significantly influenced Reynolds number with increasing temperature. Apparent viscosity also decreased significantly by increasing temperature at low shear rates. Also, transition from laminar to turbulent flow regime was accelerated by increasing temperature.

As a result, these parameters were affected by temperature and thus, this led to a change in friction pressure loss and regime transition directly. This study is the starting point of investigation of the effect of temperature on non-Newtonian fluids. It will lead to future investigations for modeling temperature effect on friction pressure loss with considering real drilling conditions including eccentricity, inclination and inner pipe rotation.

Keywords: friction pressure loss, non-Newtonian fluid, temperature, Herschel-Bulkley model, equivalent diameter

ÖZ

POLİMER BAZLI SONDAJ SIVISININ DİKEY EŞ MERKEZLİ HALKASAL ORTAMDAKİ AKIŞI SIRASINDA OLUŞAN SÜRTÜNMEYE BAĞLI BASINÇ KAYBINA SICAKLIĞIN ETKİSİNİN DENEYSEL OLARAK İNCELENMESİ

Gürçay, Kazım Onur
Yüksek Lisans, Petrol ve Doğal Gaz Mühendisliği Bölümü
Tez Yöneticisi: Prof. Dr. Serhat Akın
Eş Tez Yöneticisi: Doç. Dr. İsmail Hakkı Gücüyener

Eylül 2018, 88 sayfa

Halkasal ortamda sürtünmeye bağlı basınç kaybının doğru olarak hesaplanması, tam kaçak, takım sıkışması, formasyon sıvısının kuyu içine girmesi ve bunun gibi ciddi sondaj ve kuyu tamamlama problemlerinden kaçınmak için önemlidir. Deneysel ve teorik olarak, boru ve halkasal ortamda sürtünmeye bağlı basınç kaybı, sondaj borusunun eksantrikliği, borunun dönmesi, halkasal ortamın geometrisi ya da akış biçimi etkisi altında birçok çalışmada incelenmiştir. Tüm bu faktörlere ek olarak, sıvı reolojisi sıcaklığa bağlıdır ve reolojik özelliklerdeki değişim de sürtünmeye bağlı basınç kaybını etkilemektedir. Buna rağmen, Newtonian olmayan sıvıların akışındaki sürtünmeye bağlı basınç kaybına sıcaklığın etkisi deneysel olarak henüz araştırılmamıştır.

Bu çalışma, polianyonik selüloz (0.50 lb/bbl) ve ksantan sakızı (0.75 lb/bbl) polimerleri içeren sondaj sıvısının dikey eş merkezli halkasal ortamdaki (2.91 inç X 1.85 inç) akışı sırasında ortaya çıkan sürtünmeye bağlı basınç kaybına sıcaklığın etkisini deneysel olarak inceledi. Sürtünmeye bağlı basınç kaybı Bingham Plastic, Power Law ve Herschel-Bulkley reolojik modelleri arasında, ölçülen ile hesaplanan kayma gerilimi arasında en az hataya sahip olan Herschel-Bulkley reolojik modeli ile dört farklı eşdeğer çap tanımı kullanılarak teorik olarak hesaplandı. Çalışma da ek olarak, sürtünmeye bağlı basınç kayıplarının teorik ve deneysel sonuçları karşılaştırılarak en uygun eşdeğer çap tanımı olarak laminar akış için hidrolik yarıçap tanımı, türbülanslı akış için slot yaklaşım tanımı seçildi ve hesaplar bu tanımlara göre yeniden yapıldı.

Reolojik parametreler, Reynolds sayısı ve görünür viskoziteye sıcaklığın etkileri araştırıldı. Reolojik parametreler içinde uyumluluk endeksi ve akma noktasının, akış davranış endeksine göre sıcaklığa karşı daha hassas olduğu görüldü. Daha sonra, Reynolds sayısı ve görünür viskozitenin sıcaklığa bağlı grafikleri farklı akış hızlarında (25-125 gpm arası) değerlendirildi ve yüksek akış hızının, Reynolds sayısını sıcaklığın artışı ile ciddi şekilde etkilediği görüldü. Görünür viskozite de aynı şekilde düşük akış hızlarında daha ciddi düşüş gösterdi. Ek olarak, laminar akıştan türbülanslı akışa geçişin sıcaklıkla birlikte daha erken olduğu görüldü.

Sonuç olarak, bu parametrelerin sıcaklıktan etkilendiği görüldü ve bu yüzden bu durum sürütnmeye bağlı basınç kaybı ve akış biçimi geçişlerini doğrudan etkilemektedir. Bu çalışma Newtonian olmayan akışkanlara sıcaklığın etkisini araştıran bir başlangıç çalışmasıdır. Sıcaklığın, gerçek sondaj şartlarını gösteren diğer değişkenlerle beraber sürtünmeye bağlı basınç kaybına etkisinin modellenmesi gibi gelecek çalışmalara ışık tutacaktır.

Anahtar kelimeler: sürtünmeye bağlı basınç kaybı, Newtonian olmayan akışkan, sıcaklık, Herschel-Bulkley modeli, eşdeğer çap

to my beloved family

ACKNOWLEDGEMENTS

I wish to express my sincere gratitude to my supervisor Prof. Dr. Serhat Akın for his motivation, guidance, and the continuous support from determining the topic of thesis to the end of this research. Also, I am very grateful to him to provide all the necessary facilities to conduct experimental works.

I would like to thank my co-supervisor Assoc. Prof. Dr. İsmail Hakkı Gücüyener. His great experience, enthusiasm and determination helped me throughout the study.

GEOS Energy Inc. is also acknowledged for additive supply to perform experiments.

Furthermore, I would like to thank my friend Berk Bal for technical support and contribution during experiments.

My beloved wife Akbel Tekeli Gürçay truly deserves appreciation as she has always been next to me with her encouragement, endless support and patience. Also, I wish to thank to my parents for their warm support.

Finally, I am grateful to everyone helping me directly or indirectly.

TABLE OF CONTENTS

LIST OF FIGURES

FIGURES

LIST OF TABLES

TABLES

NOMENCLATURE

a, b	Blasius correlation constants
B_a	Well geometry correction factor
B_x	Viscometer correction factor
D	Diameter, in
D_o	Outer diameter of annulus, in
D_i	Inner diameter of annulus, in
D_{hyd}	Equivalent diameter definition of hydraulic radius, in
D_{slot}	Equivalent diameter definition of slot flow approximation, in
D_{Lamb}	Equivalent diameter definition of Lamb, in
D_{Crit}	Equivalent diameter definition of Crittendon, in
$D_{effective}$	Effective diameter, in
f	Friction factor
$f_{laminar}$	Laminar flow regime friction factor
$f_{transition}$	Transition flow regime friction factor
$f_{turbulent}$	Turbulent flow regime friction factor
$f_{intermediate}$	Intermediate friction factor
G	Combined geometry shear-rate correction factor

He	Hedstrom number
K	Consistency index of Herschel-Bulkley model, lb-sec^n/100 ft^2
K_p	Consistency index of Power Law model, lb-sec^n/100 ft^2
n	Flow behavior index of Herschel-Bulkley model
n_p	Flow behavior index of Power Law model
N_{Re}	Reynolds number
N_{ReG}	Generalized Reynolds number
$N_{CRe,L}$	Lower Critical Reynolds number
$N_{CRe,U}$	Upper Critical Reynolds number
$\frac{dP_f}{dL}$	Friction pressure loss gradient, psi/ft
Pr	Prandtl number
q	Flow rate, gpm
r	Radius, in
r_o	Outer radius of annulus, in
r_i	Inner radius of annulus, in
Ta	Taylor number
v	Velocity, ft/sec
$\bar{v}$	Average velocity, ft/sec
α	Geometry factor

γ	Shear rate, 1/sec
γ_w	Shear rate at wall, 1/sec
γ_G	Geometric mean of shear rates, 1/sec
$\gamma_{min}, \gamma_{max}$	Maximum, minimum shear rate, 1/sec
ϵ	absolute roughness, in
θ	Dial reading
μ	Viscosity, cp
μ_p	Plastic Viscosity, lb-s/100 ft^2
μ_{app}	Apparent Viscosity, lb-s/100 ft^2
ρ	Density, ppg
τ	Shear stress, lb/100 ft^2
τ_y	Yield point, lb/100 ft^2
τ_w	Shear stress at wall, lb/100 ft^2
τ_G	Shear stress corresponding to geometric mean of shear rates, lb/100 ft^2
τ_{min}, τ_{max}	Maximum, minimum shear stress, lb/100 ft^2

CHAPTER 1

INTRODUCTION

Accurate estimation of pressure loss through annulus accurately has a great importance for drilling and well completion operations for keeping the well overpressured. Any mistake on the calculation of annular pressure loss may cause serious problems which can interrupt the drilling and may even result in abandoning the well. Therefore, hydraulic programs for these operations must be precisely optimized to determine pump rates.

Hydraulic programs of geothermal and high pressure - high temperature wells are prepared without considering the effect of temperature because any analytical, numerical or empirical solutions of friction pressure loss of non-Newtonian fluids with the effect of this parameter has not been found yet. Only, the study of Ulker, Sorgun, Solmus, and Karadeniz (2017) has been found an empirical correlation for the effect of temperature on Newtonian fluids.

The main aim of the thesis is to investigate the effect of temperature on the friction pressure loss of non-Newtonian fluid through vertical concentric annulus experimentally. In addition, friction pressure loss calculations with different equivalent diameter definitions have been performed theoretically. Finally, by investigating the effect of temperature, rheological parameters, Reynolds number, and apparent viscosity were examined. This study is the starting point of wide spectrum future investigations. After this work, experiments including the effects of eccentricity and pipe rotation with temperature will be conducted, and these effects will be modeled to find the relationship between friction pressure loss and flow rate.

There have been many studies about the flow of Newtonian and non-Newtonian fluids in the annulus by considering the effects of eccentricity, pipe rotation, equivalent diameter definitions, friction factor correlations and flow patterns. About these topics, literature has been searched and summarized in the Literature Review section. Despite all of these studies, there is still a gap for the effect of temperature on the flow of non-Newtonian fluids. In Theory section, types of fluids, rheological models including Bingham Plastic, Power Law and Herschel-Bulkley, determination of these models' parameters and friction pressure loss estimation have been mentioned with different equivalent diameter definitions. Statement of the Problem part has presented the necessity of this study of temperature effect on friction pressure loss for using in real life drilling and well completion operations. Experimental Setup and Procedure part have shown the properties and photos of the equipment used in Middle East Technical University flow loop laboratory, some modification done in the lab and the procedures applied to perform experiments. In Results and Discussion part, data obtained from the experimental works have been tabulated and plotted to see the effect of temperature on friction pressure loss, Reynolds number and rheological parameters. Also, some experimental insufficiencies affecting the results have been discussed. Finally, thesis has been completed with conclusions and recommendations sections.

CHAPTER 2

LITERATURE REVIEW

Flow of non-Newtonian fluids through the pipe was investigated firstly by Metzner and Reed (1955). According to their study, they calculated the frictional pressure loss and then found the relationship between friction factor and Reynolds number by generalizing non-Newtonian fluids to equivalent Newtonian fluids and finally compared with the data obtained from previous studies of different Power Law fluids and pipe sizes. As a result, for laminar and turbulent flow, their friction factor vs. Reynolds number plot had good agreement with real data and correlations for these flow patterns were presented.

One of the first studies about non-Newtonian flow through annulus was carried out by Fredrickson and Bird (1958). They calculated frictional pressure loss by finding an analytical solution to the equation of motion for axial flow of incompressible fluids like molten plastic and drilling fluids according to Bingham Plastic and Power Law Models. However, these solutions are valid for laminar flow and only diameter ratios of more than 0.5 gives consistent frictional pressure loss values (Demirdal and Cunha ,2007).

The first study about the flow of non-Newtonian fluids under turbulent pipe flow conditions was performed by Dodge and Metzner (1959). By applying the Power Law model, they found a relationship between friction pressure loss and flow rate and then velocity profiles through pipe were represented. Also, they proposed the following correlation between friction factor and generalized Reynolds number for turbulent flow non-Newtonian fluids including polymeric gels and solid-liquid suspensions.

$$\sqrt{\frac{1}{f}} = \frac{4}{{n_p}^{0.75}} \log\left[N_{ReG} f^{\left(1-\frac{n_P}{2}\right)}\right] - \frac{0.4}{{n_P}^{1.2}} \tag{2.1}$$

Proposed equation gave good agreement when compared with experimental results with these fluids.

In order to apply equations of pipe flow to annular flow, equivalent diameter concepts have been presented. Mostly common equivalent diameter definitions are hydraulic diameter, slot flow approximation (Bourgoyne Jr., Millhelm, Chenevert, and Young Jr., 1991), Lamb’s diameter (Lamb, 1945) and Crittendon’s diameter (Crittendon, 1959). For this reason, Jensen and Sharma (1987) studied about finding the best combination of friction factor and equivalent diameter definitions in order to calculate friction pressure loss by applying Bingham Plastic and Power Law model for the flow of drilling fluids through annulus accurately by comparing with the data from two different wells. For equivalent diameter definitions, mostly common ones that are Crittendon's diameter, the hydraulic diameter, the slot flow approximation and Lamb's diameter were selected. Also, 10 different friction factor correlations were examined. Colebrook's friction factor correlation (Colebrook, 1939) that is shown below was the mostly known equation among others.

$$f = \{-2\log[\epsilon/3.7D_{eq} + 2.51/\left(N_{Re}\sqrt{f}\right)]\}^{-2} \tag{2.2}$$

According to the results, for Bingham Plastic fluids, the combination of N. H. Chen's (Chen, 1979) correlation for friction factor and the hydraulic diameter concept gave the best result. (R^2=0.969). However, new correlation was proposed for friction factor and combined with hydraulic diameter, and then this combination gave the value of 0.982 for R^2. Likewise, for Power Law fluid, Blasius's (Bourgoyne Jr. et al., 1991) friction factor correlation and hydraulic diameter showed the best combination but the new correlation was proposed again for Power Law fluid instead of Blasius's correlation with hydraulic diameter gave the value of 0.987 for R^2. Also, Colebrook' correlation for friction factor did not give accurate results despite being a most popular correlation.

Gucuyener and Mehmetoglu (1992) investigated the axial flow of yield pseudoplastic fluids in concentric annuli under laminar flow conditions. They proposed an analytical solution to the volumetric flow rate of these fluids with Robertson-Stiff rheological model and simply found pressure loss through the annulus. They continued their works with the investigation of the laminar-turbulent transition of yield pseudoplastic fluids through pipes and concentric annuli (Gucuyener and Mehmetoglu, 1996). For this reason, several criteria for transition from the laminar flow to turbulent flow were examined. Among those, Hanks' stability criterion (Hanks, 1963) was reanalyzed for concentric annular flow by studying all theoretical and experimental works of Hanks. There were two different critical values at the inner and outer region for the flow through the annulus. The outer value was always bigger than inner value, and transition took place according to outer critical modified Reynolds number. As a result, critical modified Reynolds number for yield pseudoplastic fluid flow by applying Robertson-Stiff model were found and they showed that laminar to turbulent transition was strongly related with rheology of fluids and flow geometry.

One of the most important studies has been conducted by Reed and Pilehvari (1993). They have presented a model to predict friction pressure loss through annulus for all flow regimes of drilling fluids by establishing a relationship between Newtonian pipe flow and non-Newtonian annular flow for Bingham Plastic, Power Law and Herschel-Bulkley rheological models. For this reason, they introduced a term of "Effective Diameter" that is a function of pipe geometry and type of fluid shown below. Metzner and Reed's (1955) generalized terms like Power Law exponents and Reynolds number for non-Newtonian pipe flow were extended with this effective diameter concept for laminar flow.

$$D_{effective} = D_{hydraulic}/G \tag{2.3}$$

Equation 2.3 represents the effective diameter for laminar non-Newtonian flow through concentric annuli. The parameter "G" changed with the type of fluid. Formulas for G for Power Law and Herschel-Bulkley rheological models have been presented. For turbulent flow, same equation was used with friction factor correlation proposed by Colebrook. (Colebrook, 1939) The results were compared and verified with the data obtained from experiments conducted by using mixed metal hydroxides (MMH) and bentonite drilling fluids for different pipe roughnesses in the flow loop.

Subramanian and Azar (2000) have published a paper on the flow of different non-Newtonian fluids including polymer-based drilling fluid in pipe and annulus. They used Bingham Plastic, Power Law and Yield Power Law rheological models to predict friction pressure losses for laminar and turbulent flow, and compared these results with the data from experiments conducted in their flow loop. In calculation for the concentric annulus, slot flow assumption was used and only hydraulic diameter was used as equivalent diameter. According to the results, polymer based drilling fluids showed that in laminar and turbulent flow condition, Yield Power Law model gave the best fit for concentric annulus. Also, for turbulent flow, polymer drilling fluid acted as drag reducing fluid and thus the term of pipe roughness in friction pressure loss prediction caused larger results than experiments.

Due to the complex process of friction pressure loss calculations with Herschel-Bulkley Model, Zamora, Roy, and Slater (2005) presented a unified model for Herschel-Bulkley fluids in order to predict frictional pressure losses for laminar, transition and turbulent flow through pipe and annuli. Results obtained from the model gave good agreement with the data from flow loops, full-scale yard tests and offshore wells for different annular configurations and different type of non-Newtonian fluids but some additional factors that were pipe rotation, pipe roughness, tool joints effect should be considered for more accurate results.

Demirdal and Cunha (2007) investigated the effect of different rheological models (Bingham Plastic, Low and High Shear Power Law and Yield Power Law models) and equivalent diameter concepts (slot flow approximation, Lamb's diameter, Crittendon's diameter and hydraulic radius) on the estimation of annular pressure losses in laminar flow conditions for well configurations obtained from onshore and offshore wells. Synthetic based drilling fluids were used for this study. According to results, in terms of rheological models, Bingham Plastic and High Shear Power Law Models gave the highest and lowest annular pressure losses, respectively. Also, pressure losses estimated with slot approximation and Lamb's criteria for equivalent diameter was similar to each other for all flow rates. Furthermore, when the annular space became wider, rheological models were more effective than equivalent diameter concepts for the estimation of pressure losses due to viscous forces.

Sorgun and Ozbayoglu (2010) represented a mechanistic model in order to calculate friction pressure loss for Newtonian fluids through concentric annuli in laminar and turbulent flow conditions. For this reason, the equation of motion and continuity equation were derived for turbulent, fully developed and incompressible fluid flow, and then solved numerically by using finite difference methods. A computer program was prepared for this mechanistic model. In order to compare and verify the data obtained from the proposed model and experiments conducted in flow loop located in Middle East Technical University with water, experimental results from other studies in literature, and results from CFD software simulating annular Newtonian flow and friction pressure estimation with different equivalent diameter concepts like hydraulic radius, slot flow approximation and Crittendon’s diameter were used. Model and experimental results gave good agreement, and for laminar and turbulent flow conditions, friction pressure loss for different flow rates can be calculated with 10 percent of the margin of error.

Sorgun and Ozbayoglu (2011) extended their work by investigating the flow of non-Newtonian fluids to accurately predict friction pressure loss through horizontal concentric and eccentric annulus for drilling operations. In the first part of their study, friction pressure loss was estimated by using a Eulerian-Eulerian CFD model. And then, experiments were conducted with different non-Newtonian drilling fluids containing several different concentrations of xanthan biopolymer, starch, potassium chloride, soda ash and barite as a weighting agent for different flow rates in Middle East Technical University flow loop. The last part of the study compared the results from the CFD model with different studies. Flow data was compared with those obtained from experiments and data from the literature including the friction pressure loss calculation with Power Law model with considering eccentricity by using the approach of Haciislamoglu and Langlinais (1990) and slot flow approximation in laminar and turbulent flow for drilling fluids used in experiments. All results showed that the CFD model was able to estimate friction pressure loss with an error of ±10 percent. Also, slot flow approximation gave less accurate results than the CFD model.

The studies of Ozbayoglu and Sorgun (2010) continued with the estimation of friction pressure by considering pipe rotation and eccentricity effects. A correlation including these effects was proposed and the results were compared with the data obtained from experiments. Different non-Newtonian drilling fluids that were made up of KCl-polymer and PAC were examined for different flow rates in Middle East Technical University flow loop. Also, formulas for axial and rotational Reynolds numbers were derived and used to estimate Reynolds number in the calculation of friction factor and friction pressure loss. Pipe rotation affected friction pressure loss positively for low flow rates. However, increasing flow rate did not affect friction pressure losses. Furthermore, proposed Reynolds number gave more accurate results than Dodge and Metzner's (1959) friction factor correlation.

Anifowoshe and Osisanya (2012) studied the effect of equivalent diameter concepts on friction pressure loss of helical flow of non-Newtonian drilling fluids through annuli. In their study, seven different concepts (hydraulic diameter, the slot flow approximation, Crittendon’s diameter, Lamb’s diameter, the Petroleum Engineering method, Meter and Bird’s diameter (Meter and Byron Bird, 1961) and Reed and Pilehvari’s effective diameter concept) were used. An empirical correlation of R. M. Ahmed, Enfis, El Kheir, Laget, and Saasen (2010) and the experimental data obtained from Enfis, Ahmed, and Saasen (2011) were used to find out friction pressure loss formula for Power Law model with pipe rotation in laminar flow conditions. As a result, hydraulic diameter concept gave the best agreement with experimental results in laminar flow conditions.

Dosunmu and Shah (2015) proposed a new effective diameter concept including the effect of flow geometry and rheology under laminar flow conditions. Also, for the fully eccentric flow of Power Law fluids through annulus in turbulent flow, friction factor correlation with the effects of generalized Reynolds number, diameter ratio and relative roughness was represented. Experiments were performed with different concentrations of two different polymeric fluids including guar gum and welan gum and one surfactant based fluid that was used in hydraulic fracturing operations. Laminar and turbulent results for concentric and eccentric annulus from experiments were compared with previous studies and showed good agreement.

Rooki (2015) presented an artificial neural network method to estimate pressure losses of Herschel-Bulkley fluids through annulus in terms of eccentricity. Input layer of method consisted of diameter ratio, eccentricity, Herschel-Bulkley parameters for fluid and flow rate. Results obtained from this method were compared and verified with experimental data from Ahmed's study with different polymerized drilling fluids (including XCD polymer and PAC), and different annular configurations and eccentricities. In Ahmed's study, temperature of the system reached up to 113˚F (45˚C). However, temperature effect has not considered for friction pressure loss calculations. (R. Ahmed, 2005)

Ulker et al. (2017) investigated the effect of temperature on friction pressure loss of Newtonian fluid through fully eccentric annuli with pipe rotation experimentally and presented an empirical correlation for estimation of friction pressure loss. Experiments were conducted with water by changing the temperature between 20 to 65˚C and pipe rotation between 0 to 120 rpm. By using Reynolds number and Taylor number, helical annular flow was examined and Prandtl number was taken into account to show the effect of temperature. As a result, following equation was proposed for estimating annular pressure loss.

$$\frac{dP_f}{dL} = 2 * 10^{-6} Re^{1.74} * e^{7*10^{-9} Ta} * Pr^{0.57} \qquad (2.4)$$

In conclusion, literature review showed that friction pressure loss through annulus was investigated theoretically and experimentally in different conditions. Studies have always become more complicated than previous ones. Types of fluids, eccentricity of pipe, pipe rotation, pipe roughness, different equivalent diameter definitions, friction factor correlations and flow patterns affected friction pressure loss. However, the effect of temperature has not been considered yet and study from Ulker et al. demonstrated this effect on Newtonian fluids. For non-Newtonian fluid, neither theoretical nor experimental works have been conducted in the annulus in literature.

CHAPTER 3

THEORY

The aim of this chapter is to briefly describe classification of fluids and rheological models, determination of parameters of rheological models and estimation of friction pressure losses for different rheological models by considering the effect of annular geometry.

3.1 Classification of Fluids

Fluids can be characterized as mainly Newtonian and non-Newtonian based on their rheological properties. Unlike Newtonian fluids, non-Newtonian fluids give different viscosity values under the effects of temperature and pressure.

3.1.1 Newtonian Fluids

Newtonian fluids are the base fluids of most of the drilling fluids (water, diesel oil, synthetics). For these fluids, there is no need to yield stress to initiate flow and shear stress is directly proportional to shear rate.

3.1.2 Non-Newtonian Fluids

Due to the complex nature of these fluids, shear stress of non-Newtonian fluids does not have direct proportionality with shear rate. This relationship varies with the time-independent behavior of non-Newtonian fluids. For example, shear thinning behavior is seen in drilling fluids. These fluids' viscosity decreases with increasing shear rate. In addition, dilatant behavior of non-Newtonian fluids shows that viscosity increases with increasing shear rate. Another behavior of non-Newtonian fluids is viscoplastic. In order to start to move these fluids, yield stress should be exceeded for viscoplastic fluids. (American Petroleum Institute (API), 2009) In Figure 3.1 types of time-independent fluids are given.

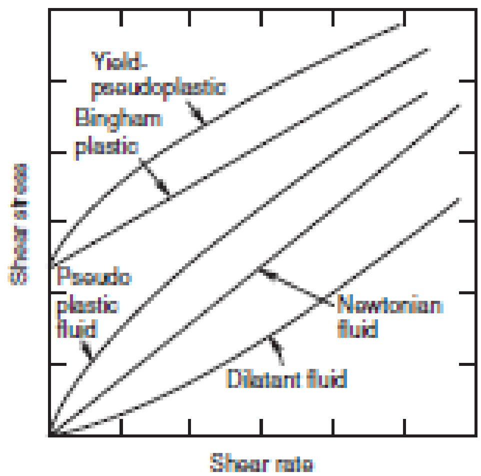

Figure 3.1 Types of Time-independent Fluid Behavior (Chhabra and Richardson, 2008)

Dependence on time effect on non-Newtonian fluids can be classified as thixotropic and rheopectic. Drilling fluids and cement slurries are thixotropic fluids. Thixotropic fluids that exhibit decreasing viscosity with time while rheopectic exhibit an increase in viscosity with time under constant shear rate. (Bourgoyne Jr. et al., 1991) (Figure 3.2)

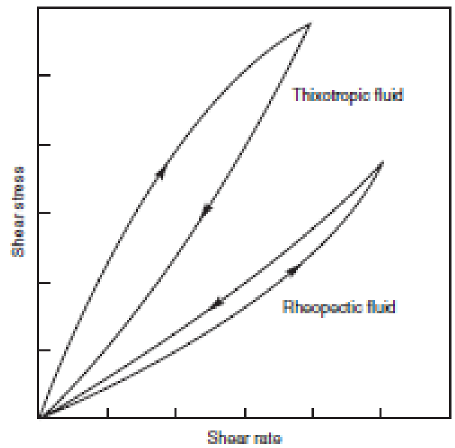

Figure 3.2 Shear Stress – Shear Rate Behavior of Time-dependent Behavior (Chhabra and Richardson, 2008)

3.2 Rheological Models

Rheological models are mostly used to identify the behavior of any fluids. They differ from each other by the methods to explain shear stress-shear rate relationships of fluids mathematically. This study focuses on four of all models in the literature. These models are Newtonian model for Newtonian fluids, and Bingham Plastic, Power Law and Herschel-Bulkley rheological models for non-Newtonian fluids. (Figure 3.1) Understanding the rheological models are important since shear stresses and friction pressure losses through pipe or annuli are predicted with these models. (Okafor and Evers, 1992)

3.2.1 Newtonian Model

Newtonian model describes the behavior of Newtonian fluids. In other words, shear stress that is applied to the fluid is directly proportional to shear rate. The slope of the shear stress-shear rate plot gives the dynamic viscosity. As a result, general equation of Newtonian model becomes:

$$\tau = \mu\gamma \tag{3.1}$$

3.2.2 Bingham Plastic Model

Bingham Plastic model is one of the most widely used rheological models. This two-parameters model describes the behavior of non-Newtonian fluids with the direct proportionality of shear stress and shear rate in excess of the yield stress. The equation of the model is shown below:

$$\begin{gathered} \tau = \tau_y + \mu_p \gamma \; ; \; \tau > \tau_y \\ \gamma = 0 \; ; \; +\tau_y \geq \tau \geq -\tau_y \\ \tau = \mu_p \gamma - \tau_y \; ; \; \tau < -\tau_y \end{gathered} \tag{3.2}$$

According to Bingham Plastic model, fluids cannot flow until shear stress reaches yield stress value. After reaching, the slope of the linear plot of shear stress and shear rate gives the plastic viscosity (μ_p).

3.2.3 Power Law Model

Power Law model is another widely used two-parametered model. This model gives straight line between shear stress and shear rate when plotting on a log-log graph and describes the behavior of non-Newtonian fluids with flow behavior index (n_p) consistency index (K_p) Power model is defined by the formula:

$$\tau = K_p |\gamma|^{n_p - 1} \gamma \tag{3.3}$$

The constant “n” characterize the behavior of the fluid. Power Law model is used for pseudoplastic fluids when “n” is smaller than 1, Newtonian fluids when “n” is equal to 1 and dilatant fluids when n is bigger than 1. (Figure 3.3) (Rabia, 2001)

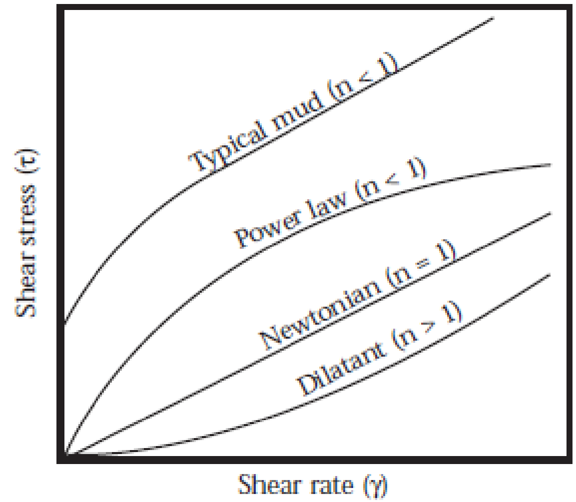

Figure 3.3 Effect of Flow Behavior Index on Fluid Behavior (MI Swaco, 1998)

3.2.4 Herschel - Bulkley Model

Herschel-Bulkley model can be called as Modified or Yield Power Law model. This model describes the behavior of non-Newtonian fluids more accurately with 3 parameters by combining Bingham Plastic and Power Law model in one mathematical expression:

$$\tau = \tau_y + K\gamma^n \tag{3.4}$$

Like Bingham Plastic model, this model has yield stress parameter in order to initiate flow of non-Newtonian fluids. Also, there are flow behavior index and consistency index like Power Law model. Herschel-Bulkley model can be Newtonian, Bingham Plastic or Power Law model by changing parameters. For example, when n=1, K=μ, and τy=0, it represents Newtonian fluid; when n=1, and τy=0, it represents Power Law fluid; and K=μp, τy=YP, and n=1, it represents Bingham Plastic fluid. Thanks to considering shear thinning behavior and yield stress, Herschel-Bulkley model is a precise model to describe most of drilling fluids shown in Figure 3.3 as typical mud.

3.3 Determination of Rheological Parameters

Our study has also investigated the effect of temperature on parameters of these models to find a way to describe temperature effect on friction pressure loss. For this reason, it is important to determine the parameters of models that are interested.

Calculation of model parameters is summarized for Bingham Plastic, Power Law and Herschel-Bulkley rheological models. (American Petroleum Institute (API), 2009) In addition to these determination methods, parameters can be found with the relationship measured shear stresses and shear rates.

3.3.1 Bingham Plastic Model

This model calculates the yield point and plastic viscosity parameters shown in Equation 4.2 by using 600 rpm and 300 rpm dial readings with the formula below.

$$Plastic\ Viscosity\ (\mu_p) = \theta_{600} - \theta_{300} \tag{3.5}$$

$$Yield\ Point\ (\tau_y) = \theta_{300} - \mu_p \tag{3.6}$$

Also, the general formula of Bingham-Plastic model shown in Equation 3.2 is used to determine these parameters. Relationship between shear stress and shear rate is found with the plot of measured shear stress and shear rates. The slope of the line represents plastic viscosity and the point intersecting x-axis gives yield point. (MI Swaco, 1998)

3.3.2 Power Law Model

There are two different equations to calculate the flow behavior index (n_p) and consistency index (K_p) for pipe and annular flow. Only at high shear rates, the values of pipe and annulus are accepted as equal. (Bourgoyne Jr. et al., 1991)

For pipe flow,

$$Flow\ behavior\ index\ (n_p) = 3.32 \log_{10}\left(\frac{\theta_{600}}{\theta_{300}}\right) \tag{3.7}$$

$$Consistency\ index\ (K_p) = \frac{\theta_{300}}{511^{n_p}} \tag{3.8}$$

For annular flow,

$$Flow\ behavior\ index\ (n_p) = 0.657 \log_{10}\left(\frac{\theta_{100}}{\theta_3}\right) \tag{3.9}$$

$$Consistency\ index\ (K_p) = \frac{\theta_{100}}{170.3^{n_p}} \tag{3.10}$$

Due to exponential relationship of shear stress and shear rate of Power Law fluids, taking the logarithm of those and then plotting in Cartesian graph gives straight line. The slope of line represents flow behavior index (n_p) and the point intersecting x-axis gives the logarithm of consistency index (K_p). (MI Swaco, 1998)

3.3.3 Herschel-Bulkley Model

Three parameters of Herschel-Bulkley model are determined by following formulas. Yield stress in this model is known as low shear rate shear stress and calculated with 3 rpm and 6 rpm dial readings of viscometer. Also, flow behavior index and consistency index are calculated by adding yield point parameters into the equation of Power Law model.

$$Yield\ Point\ (\tau_y) = 2\theta_3 - \theta_6 \tag{3.11}$$

$$Flow\ behavior\ index\ (n) = 3.32 \log_{10}\left(\frac{\theta_{600} - \tau_y}{\theta_{300} - \tau_y}\right) \tag{3.12}$$

$$Consistency\ index\ (K) = \frac{\theta_{300} - \tau_y}{511^{n}} \tag{3.13}$$

Herschel-Bulkley model is more different in determination of parameters than Bingham Plastic and Power Law models since it has three parameters. Therefore, the general formula of this model (Equation 3.4) is linearized by taking the logarithm of both sides of the equation.

$$\log(\tau - \tau_y) = \log K + n \log \gamma \tag{3.14}$$

When $\log(\tau - \tau_y)$ vs $\log \gamma$ is plotted in Cartesian graph, the slope of the straight line gives flow behavior index and this straight line intersects x-axis at the point of logarithm of consistency index. (Kelessidis, Maglione, Tsamantaki, and Aspirtakis, 2006) However, yield point is necessary to plot this graph. The method of Gucuyener (1983) can be used to find yield point. For this reason, geometric mean of shear rates (γ_G) is calculated by minimum (γ_{min}) and maximum (γ_{max}) shear rates firstly and corresponding shear stress (τ_G) is found for this shear rate.

$$\gamma_G = \sqrt{\gamma_{min} \cdot \gamma_{max}} \tag{3.15}$$

Finally, yield stress is calculated with the formula below:

$$\tau_y = \frac{{\tau_G}^2 - \tau_{min} \cdot \tau_{max}}{2\tau_G - \tau_{min} - \tau_{max}} \tag{3.16}$$

3.4 Friction Pressure Loss in Annuli

As it is stated in previous sections, friction pressure loss is one of the main issues in drilling or well completion operations in order to avoid problems arising from inaccurately prepared hydraulic programs.

In estimation of friction pressure loss in annuli, equation for pipe flow is applied to annular flow by defining equivalent diameter concepts. (Reed and Pilehvari, 1993) One of the main aim of this study was to select the most convenient equivalent diameter in friction pressure loss calculation.

The first and mostly known equivalent diameter definition is *hydraulic radius* concept that is shown below. It is calculated by four times cross-sectional area of annulus-wetted perimeter ratio. (Bourgoyne Jr. et al., 1991)

$$D_{hyd} = 4 * \frac{(\pi/4)\left({D_o}^2 - {D_i}^2\right)}{\pi(D_o + D_i)} = D_o - D_i \tag{3.17}$$

The second definition has been represented by *Lamb* to explain the friction pressure loss for laminar flow of Newtonian fluids by considering the flow system as shell of fluid having radius r. (Lamb, 1945)

$$D_{Lamb} = {D_o}^2 + {D_i}^2 - \frac{\left({D_o}^2 - {D_i}^2\right)}{\ln(D_o/D_i)} \tag{3.18}$$

Another equivalent diameter definition is *slot flow approximation*. This definition has been found by comparing different friction pressure loss estimation methods by representing annulus as a circular and rectangular slot. This concept is applied to annular geometries having more than 0.3 of the ratio of inner to outer diameter. (Bourgoyne Jr. et al., 1991)

$$D_{slot} = 0.816(D_o - D_i) \tag{3.19}$$

The last definition has been expressed by *Crittendon* empirically by investigating about a hundred different field case in fracturing applications. (Crittendon, 1959)

$$D_{Crit} = \frac{1}{2}\left(\sqrt[4]{{D_o}^4 - {D_i}^4 - \frac{\left({D_o}^2 - {D_i}^2\right)^2}{\ln(D_o/D_i)}} + \sqrt{{D_o}^2 - {D_i}^2}\right) \tag{3.20}$$

3.4.1 Determination of Friction Pressure Loss in Annuli

Friction pressure loss calculations through concentric annuli are shown in this section model by considering rheological models for different flow regimes. Newtonian, Bingham

Plastic and Power Law models were taken from Applied Drilling Engineering (Bourgoyne Jr. et al., 1991), and then, Herschel-Bulkley model was solved with methods given in American Petroleum Institute Recommended Practices 13D: Rheology and Hydraulics of oil-well drilling fluids (American Petroleum Institute (API), 2009) by considering concentric annuli. .

3.4.1.1 Newtonian Model

Friction pressure loss can be found by applying Newton's law of motion to shell of fluid having radius r. The general equation obtained from this method is:

$$\tau = \frac{r}{2}\frac{dP_f}{dL} + \frac{C}{r} \tag{3.21}$$

where C is the integration constant.

Formula stated above is solved for Newtonian model by combining general shear stress-shear rate relationship of Newtonian fluids expressed in Equation 3.1.

$$\tau = -\mu\frac{dv}{dr} = \frac{r}{2}\frac{dP_f}{dL} + \frac{C}{r} \tag{3.22}$$

Velocity obtained from equation by integrating:

$$v = -\frac{r^2}{4\mu}\frac{dP_f}{dL} + \frac{C}{\mu}\ln r + C_1 \tag{3.23}$$

where C_1 is second integration constant.

Equation 4.15 is solved for the boundary conditions representing annulus (r_2=inner radius of outer pipe; r_1=outer radius of inner pipe).Finally, velocity becomes:

$$v = \frac{1}{4\mu}\frac{dP_f}{dL}\left[(r_2{}^2 - r^2) - (r_2{}^2 - r_1{}^2)\frac{\ln r_2/r}{\ln r_2/r_1}\right] \tag{3.24}$$

In order to find the relationship between friction pressure loss and flow rate, flow rate is considered as the total flow of each fluid shell:

$$q = \int v(2\pi r)dr \tag{3.25}$$

Equation 4.16 is substituted to Equation 3.17 and integrated. Then flow rate is represented as:

$$q = \frac{\pi}{8\mu}\frac{dP_f}{dL}\left[(r_2{}^4 - r_1{}^4) - \frac{(r_2{}^2 - r_1{}^2)^2}{\ln r_2/r_1}\right] = \pi(r_2{}^2 - r_1{}^2)\bar{v} \tag{3.26}$$

As a result, friction pressure loss equation demonstrated below is derived in terms of field units:

$$\frac{dP_f}{dL} = \frac{\mu\bar{v}}{1500\left(D_o{}^2 + D_i{}^2 - \frac{\left(D_o{}^2 - D_i{}^2\right)^2}{\ln D_o/D_i}\right)} \tag{3.27}$$

This equation has been derived by Lamb. (Lamb, 1945) Denominator of this formula represents equivalent diameter definition of Lamb. Instead of Lamb's diameter, other equivalent diameter definitions can be used for Newtonian laminar flow and equation becomes:

$$\frac{dP_f}{dL} = \frac{\mu\bar{v}}{1500\left(D_{eq}\right)^2} \tag{3.28}$$

Same equation is obtained by representing annulus as a rectangular slot. When slot flow approximation is used as equivalent diameter, the general formula of this representation is found.

Average velocity through annulus is calculated with formula below:

$$\bar{v} = \frac{q}{2.448\left(D_o{}^2 - D_i{}^2\right)} \tag{3.29}$$

Average velocity is used for all equivalent diameter definition except Crittendon's diameter. When Crittendon's diameter is used, in equation 3.21, $\left(D_o{}^2 - D_i{}^2\right)$ is replaced with $D_{Crit}{}^2$. (Jensen and Sharma, 1987)

For turbulent flow, firstly, dimensionless Reynolds number is necessary to determine the onset of turbulence. Equation of Reynolds number for annular flow is:

$$N_{Re} = \frac{928\rho\bar{v}D_{eq}}{\mu} \tag{3.30}$$

If Reynolds number exceeds 2100, flow regime is accepted as turbulent. Friction pressure loss in turbulent conditions is estimated empirically by adding the parameter of friction factor. The relationship between friction factor and Reynolds number has been presented by Colebrook (Colebrook, 1939):

$$\frac{1}{\sqrt{f}} = -4\log(0.269\,\epsilon/D + \frac{1.255}{N_{Re}\sqrt{f}}) \tag{3.31}$$

For smooth pipes ($\epsilon/D = 0$) and $2100 \leq N_{Re} \leq 100000$, Blasius has proposed following equation:

$$f = \frac{0.0791}{{N_{Re}}^{0.25}} \tag{3.32}$$

Finally, friction pressure loss equation for annular turbulent flow in terms of field units becomes:

$$\frac{dP_f}{dL} = \frac{f\rho\bar{v}^2}{25.8D_{eq}} \tag{3.33}$$

3.4.1.2 Bingham Plastic Model

Friction pressure loss for Bingham Plastic model in laminar flow condition is found by applying the similar procedure of Newtonian model by using general Bingham Plastic model equation (Equation 3.2).

$$\frac{dP_f}{dL} = \frac{\mu_p\bar{v}}{1500\left(D_{eq}\right)^2} + \frac{\tau_y}{225D_{eq}} \tag{3.34}$$

The onset of turbulence in Bingham Plastic model is determined by using two criteria. The first criterion is that turbulence begins when Reynolds number exceeds 2100. Reynolds number is calculated with Equation 3.22. Apparent viscosity term shown below is used in general formula of Reynolds number.

$$\mu_{app} = \mu_p + \frac{6.66\tau_y D_{eq}}{\bar{v}} \tag{3.35}$$

The second criterion is to examine Hedstrom number. This number is given as:

$$He = \frac{37100\rho\tau_y {D_{eq}}^2}{{\mu_p}^2} \tag{3.36}$$

By using Hedstrom number chart, critical Reynolds number is found. This critical number is compared with calculated Reynolds number by using Equation 3.22 with plastic viscosity.

After deciding that flow regime is turbulent, friction factor is determined with Colebrook function and then, friction pressure loss is found by using Equation 3.25.

3.4.1.3 Power Law Model

Friction pressure loss through annulus for Power Law model in laminar flow condition is calculated by using this formula:

$$\frac{dP_f}{dL} = \frac{K_P \bar{v}^{n_p}}{144000\left(D_{eq}\right)^{1+n_p}} \left(\frac{3 + 1/n_p}{0.0416}\right)^{n_p} \tag{3.37}$$

Laminar to turbulent flow regime transition occurs when Reynolds number reaches to 2100. To calculate the Reynolds number, apparent viscosity used in Equation 3.22 is shown below.

$$\mu_{app} = \frac{K_P d^{(1-n_p)}}{96\bar{v}^{1-n_p}} \left(\frac{3 + 1/n_p}{0.0416}\right)^{n_p} \tag{3.38}$$

Colebrook correlation does not give accurate results in Power Law model. Thus, Dodge and Metzner, 1959 correlation is used to determine friction factor.

$$\sqrt{\frac{1}{f}} = \frac{4}{{n_p}^{0.75}} \log\left[N_{Re} f^{\left(1-\frac{n_p}{2}\right)}\right] - \frac{0.395}{{n_p}^{1.2}} \tag{3.39}$$

Friction pressure loss in turbulent flow regime is calculated with Equation 4.25

3.4.1.4 Herschel – Bulkley Model

Formulas of friction pressure loss for Herschel-Bulkley rheological model has been derived empirically in API RP 13D for rheology and hydraulics of oil-well drilling fluids (2009) in laminar, transition and turbulent flow regimes. (American Petroleum Institute (API), 2009)

Velocity of fluids through annuli is the first parameter to calculate. Following equation represent velocity of fluid in the unit of ft/min:

$$\bar{v} = \frac{24.51q}{\left({D_o}^2 - {D_i}^2\right)} \tag{3.40}$$

In order to find generalized Reynolds number defined by Metzner and Reed (1955) used for both pipe and annuli, shear rate and shear stress at pipe wall is necessary. Therefore, shear rate correction for well geometry to separate pipe and annular flow and viscometer correction are conducted.

Geometry correction factor is formulated below:

$$B_a = \left[\frac{(3-\alpha)n+1}{(4-\alpha)n}\right]\left[1+\frac{\alpha}{2}\right] \tag{3.41}$$

Geometry factor, α is accepted as 1 for annular flow.

Viscometer correction factor (B_x) is accepted as 1 for Herschel-Bulkley fluids. As a results, combined geometry shear rate correction factor is calculated by using equation given as:

$$G = \frac{B_a}{B_x} \cong B_a \tag{3.42}$$

With this factor, shear rate is determined.

$$\gamma_w = \frac{1.6GV}{D_{eq}} \tag{3.43}$$

After that, shear stress at wall is calculated by combining general Herschel-Bulkley equation with geometry factor. Equation is shown as:

$$\tau_w = 1.066 \left(\frac{4-\alpha}{3-\alpha}\right)^n \tau_y + K{\gamma_w}^n \tag{3.44}$$

Apparent viscosity of the fluid is determined by dividing wall shear stress to wall shear rate. (Reed and Pilehvari, 1993) Then, generalized Reynolds number is calculated with the following equation:

$$N_{ReG} = \frac{\rho \bar{v}^2}{19.36\tau_w} \tag{3.45}$$

In order to determine the lower critical Reynolds number for laminar to transition flow regime, flow behavior index is used.

$$N_{CRe,L} = 3470 - 1370n \tag{3.46}$$

Upper critical Reynolds number is defined by Schuh (1965) for transition to turbulent flow regime.

$$N_{CRe,U} = 4270 - 1370n \tag{3.47}$$

After calculating Reynolds number, friction factor is estimated by combining the generalized Reynolds number, rheological parameters and flow regimes.

For laminar flow, friction factor is calculated as:

$$f_{laminar} = \frac{16}{N_{ReG}} \tag{3.48}$$

For transitional flow,

$$f_{trans} = \frac{16N_{ReG}}{{N_{CRe,L}}^{2}} \tag{3.49}$$

For turbulent flow, Blasius' correlation for Power Law model is used.

$$f_{turbulent} = \frac{a}{{N_{ReG}}^{b}} \tag{3.50}$$

where

$$a = \frac{\log n_p + 3.93}{50} \qquad b = \frac{1.75 - \log n_p}{7} \tag{3.51}$$

By using friction factors of laminar, transitional and turbulent flow regimes, general friction factor for all regimes is calculated with the equation shown below:

$$f = \left({f_{int}}^{12} + {f_{laminar}}^{12}\right)^{1/12} \tag{3.52}$$

where

$$f_{int} = \left({f_{trans}}^{-8} + {f_{lurbulent}}^{-8}\right)^{8} \tag{3.53}$$

As a result, friction pressure loss is determined with the given formula:

$$\frac{dP_f}{dL} = \frac{1.076\rho\bar{v}^2 f}{10^5 D_{eq}} \tag{3.54}$$

CHAPTER 4

STATEMENT OF THE PROBLEM

Friction pressure loss is an important parameter for hydraulic program of any well. Factors affecting friction pressure loss other than temperature have already been investigated by several researchers. Also, for Newtonian Fluids, a correlation has been proposed for this effect by using dimensionless parameters. However, temperature effect has not just been a topic of any research for non-Newtonian fluids.

The primary aim of this study is to investigate the effect of temperature on friction pressure loss for non-Newtonian fluids through vertical concentric annuli, since, this is a requirement for drilling in geothermal and HPHT conditions. For this reason, firstly, the effect of temperature was investigated experimentally by measuring friction pressure loss and flow rates and then, friction pressure loss was estimated by applying the most suitable rheological model by considering average error, standard deviation and coefficient of correlation. And then, theoretical and experimental friction pressure loss results were compared in order to find the most appropriate equivalent diameter definition. Finally, model parameters, apparent viscosity and Reynolds number have been examined to see the temperature effect.

CHAPTER 5

EXPERIMENTAL SETUP AND PROCEDURE

Experiments were performed at flow loop laboratory of Middle East Technical University Department of Petroleum and Natural Gas Engineering. This laboratory has equipment that are mainly liquid suction and collection tanks, centrifugal pumps, valves to control flow, flow meter, pressure transmitter and computer program to monitor and save the data.

The aim of the experimental study is to observe the effect of temperature on friction pressure loss of the flow of water and polymeric drilling fluid including Polyanionic Cellulose (PAC HV) and Xanthan Gum through the vertical concentric annulus. Therefore, experiments were divided into two categories:

1- Water experiments
2- Polymeric drilling fluid experiments.

5.1 Experimental Setup

METU PETE Flow loop was modified before conducting experimental works. These modifications are listed below.

1- Annular test section was brought to a vertical position on its movable corner with the help of the pulley.
2- In order to increase and monitor the temperature of fluids, resistances and thermocouples were mounted to suction and cuttings tanks. Also, another

thermocouple was mounted to annular test section and connected to a computer to monitor the temperature of the test section.

3- Two centrifugal mud pumps' scroll sections were cleaned and fixed to get maximum performance from the pumps.

4- Since cutting transport were not investigated in experiments, cutting tanks and lines, and shale shaker were not used and then, return line of fluids was diverted directly to suction tank.

After all of these modifications, experimental setup was ready to operate. The schematic of the flow loop is shown in Figure 5.1.

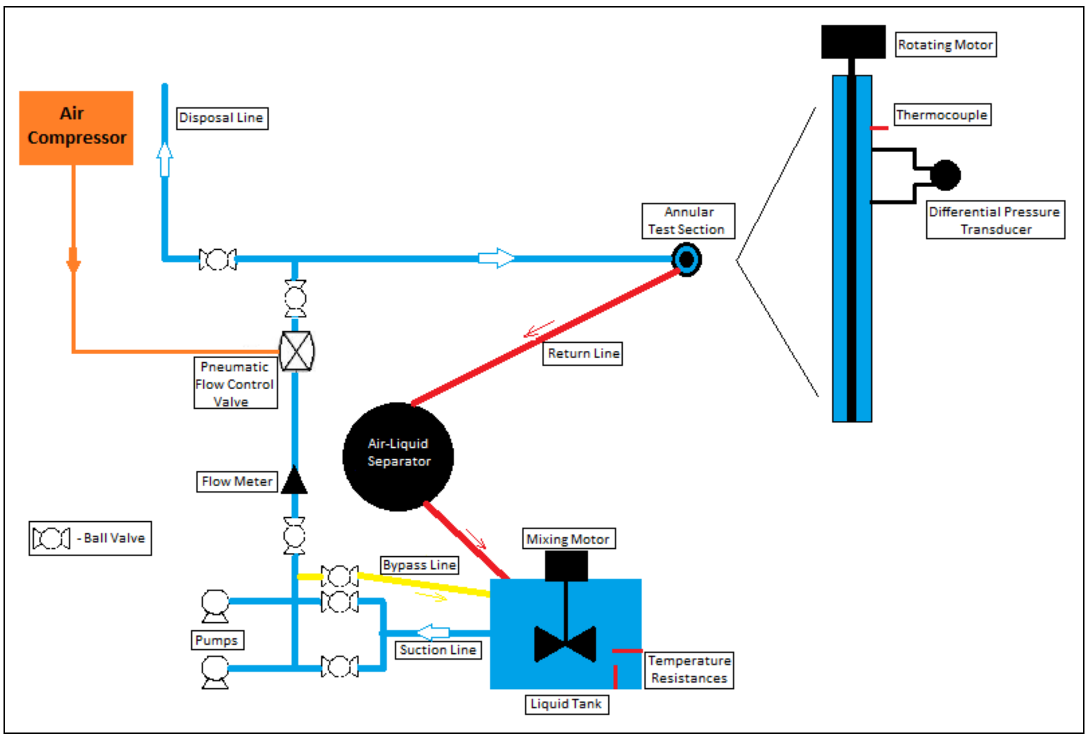

Figure 5.1 Schematic of Flow Loop

Flow loop has a 21-ft long annular test section including 2.91" ID transparent pipe with 1.85" OD drill pipe sections demonstrated in Figure 5.2. Eccentricity and rotation speed of inner pipe can be adjusted. Also, inclination of the pipe is also adjusted from 0 to 90 degree with a movable corner. In this study, experiments were conducted through a vertical concentric test section with no rotation.

Figure 5.2 Vertical Annular Test Section

Fluids are prepared at suction tank that has the capacity of 2000 liters. Suction tank is equipped with mixer and temperature resistances. (Figure 5.3) After reaching desired temperature, with the help of the thermostat, temperature could be kept constant during experiment.

Figure 5.3 Mixing motor and Resistances

Fluids prepared in the tank are pumped to the annular test section with two parallel centrifugal pumps (Figure 5.4), and circulated through the system. The flow rate control of fluids is provided by a pneumatic valve that adjusted flow rate remotely. (Figure 5.5).

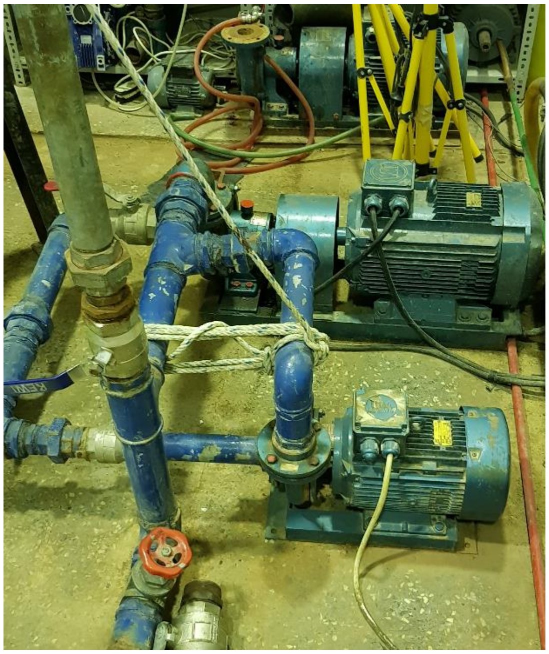

Figure 5.4 Mud Pumps

Figure 5.5 Pneumatic Flow Control Valve

Air is pumped to operate the pneumatic valve by an air compressor. (Figure 5.6) Also, flow rate is measured by a magnetic flow meter located between pumps and pneumatic valve. (Figure 5.7)

Figure 5.6 Air Compressor

Figure 5.7 Flow meter

There are two pressure taps on annular test section directly enter to pressure transmitter (Figure 5.8) in order to measure the friction pressure loss of 1 ft section through the annulus. In this study, lower tap was positioned at 14.9 ft from inlet, and upper tap was located at 5.1 ft from outlet to keep away from end effect and get data from fully developed section. Lines from the test section and fresh water tap are controlled at the manifold with several valves. The duties of manifold are to remove air and any contaminants from transmitter with fresh water and to equalize pressure after conducting experiments.

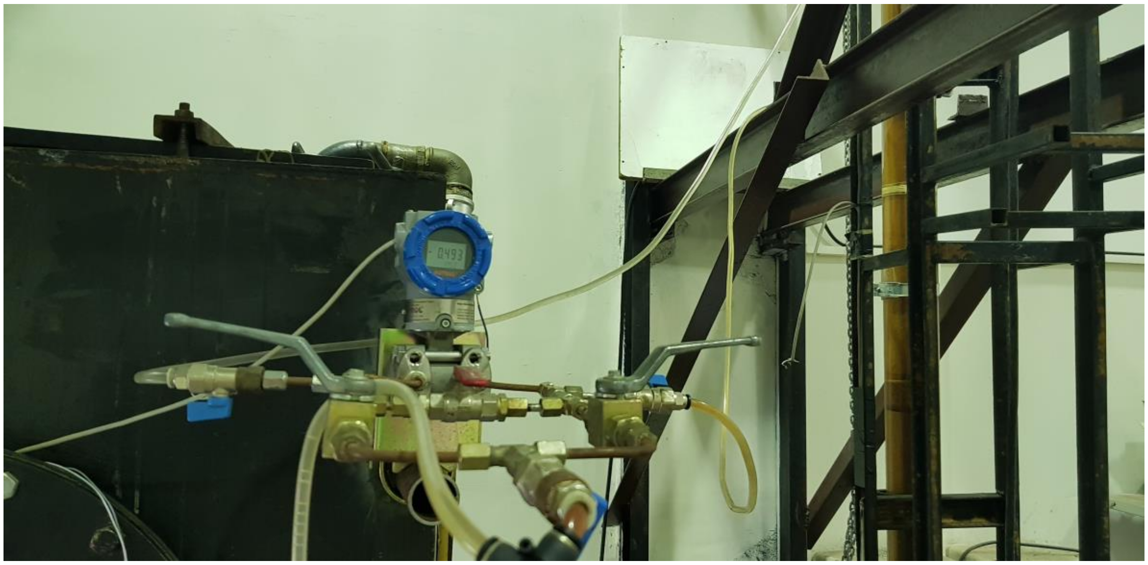

Figure 5.8 Pressure Transmitter

Dial readings at different shear rates are measured with Viscometer shown in Figure 5.9. In this experiments, dial readings and temperature were measured before pumping to system and after returning to the liquid tank at steady state.

Figure 5.9 Viscometer

Pressure transmitter and flow meter are connected to National Instrument NI SCXI-1303 data logger that is located next to the computer. (Figure 5.10)

Figure 5.10 Data Logger

LabVIEW 2013 software is used to monitor and save the data obtained from the data logger during experiments. LabVIEW front panel prepared during previous studies performed in this laboratory was used in this study. (Figure 5.11) For accurate measurement, calibration checks were conducted regularly.

Figure 5.11 LabVIEW Front Panel

The capacity and brand name of equipment in the flow loop are listed in the table below.

Table 5.1 Brand Name and Capacity of Equipment in Laboratory

Equipment	Brand Name	Capacity
Air Compressor	SETKOM SVK 30	3650 lt/min at 8 bar
Centrifugal Pumps	DOMAK	1.136 m^3/min
Liquid Tank		2000 m^3
Magnetic Flow Meter	TOSHIBA	1.136 m^3/min
Differential Pressure Transducer	AUTROL APT 3100	0 – 5 psi
Electro Pneumatic Control Valve	SAMSON	
Viscometer	FANN 35SA	

5.2 Procedure

All experiments were started to perform at ambient temperature (about 25°C) and atmospheric pressure. After that, temperature of the system was increased gradually up to about 45°C. For conducting experiments, annular test section was positioned vertically, and inner drill pipe was not rotated. To maintain the accuracy of measurements, equipment was calibrated regularly. As mentioned previously, experiments were divided into two section named as water and polymeric drilling fluid experiments.

5.2.1 Water Experiments

Following procedures were applied for investigating the temperature effect on Newtonian fluids through vertical concentric annulus.

1. Liquid tank is filled with water by measuring the volume of water with flow meter located in fresh water tap.
2. All valves are controlled to maintain the flow from selected pump to annular test section.
3. Air compressor is opened to control pneumatic flow control valve.
4. Computer and then LabVIEW Software is turned on.
5. Differential pressure transducer lines are flushed with water to prevent air bubbles.
6. Pump is started.
7. Flow rate is adjusted by opening pneumatic flow control valve until reaching desired value, and it is waited to stabilize in this value.
8. Data are started to record.
9. Flow rate is changed for another desired value and same procedures are applied.
10. After recording sufficient data, recording is stopped.
11. Pump is stopped.
12. Temperature resistances are turned on and adjusted to desired temperature value.
13. It is waited until reaching desired value. During heating up, mixer is turned on to equalize temperature in liquid tank.
14. Differential pressure transducer lines are flushed with water to prevent air bubbles.
15. Pump is started.
16. It is waited to stabilize inlet and outlet temperature values.

17. After reaching desired temperature value, flow rate is adjusted by opening pneumatic flow control valve until reaching desired flow rate value, and it is waited to stabilize in this value.
18. Same steps (8 to 17) are applied for all temperature values.
19. Pump and then air compressor are stopped after all experiments are conducted.

Test matrix for water experiments is shown Table 5.2.

Table 5.2 Test Matrix for Water Experiments

	Minimum – Maximum
Average Liquid Flow Rate	40 – 110 gpm
Temperature	20 – 45°C

5.2.2 Polymeric Drilling Fluid Experiments

Polymeric drilling fluid experiments are categorized as drilling fluid preparation and experiments.

5.2.2.1 Fluid Preparation

Polymeric drilling fluid was prepared with REOPAC HV (Polyanionic Cellulose) and REOZAN D (Xanthan Gum) provided by GEOS Energy Inc (Figure 5.12).

Figure 5.12 Drilling Fluid Additives

REOPAC HV is used as viscosifier and fluid loss control additive, and REOZAN D is used as viscosifier in industry. Before starting experimental works in flow loop, the amount of these additives were determined as 0.50 and 0.75 lb/bbl for REOPAC HV and REOZAN D, respectively in Middle East Technical University Department of Petroleum and Natural Gas Engineering Drilling Fluid Laboratory. Physical properties of these additives taken from GEOS Energy Inc. are listed below.

Table 5.3 Physical Properties of Additives

	REOZAN-D	REOPAC HV
Appearance	Cream colored powder	White powder
pH	6-8 (1% solution)	7-8 (1% solution)
Bulk Density (kg/m^3)	650-900	600-800

Following procedures were applied for preparation of drilling fluid.

1. Liquid tank is filled with water (1200 lt).
2. Mixer is turned on.

3. Pump is started and flow is directed to bypass line to avoid occurring fisheye during polymeric fluid preparation.
4. REOPAC HV and REOZAN D are added to the water very slowly in amount of 0.10 lb/bbl, respectively.
5. After adding desired amount of these additives, dial readings are measured and recorded.
6. In order to control the bacteria growth in the tank while waiting, 1.5 lt of GEOCIDE T (Triazine based biocide) provided by GEOS Energy Inc. was added to the tank (Figure 5.13).

Figure 5.13 Additive for Bacteria Growth Control

5.2.2.2 Experiments

Same procedure was applied for examining the temperature effect on polymeric drilling fluid through concentric annuli. The only difference from water experiments was to measure dial readings for all stabilized temperature value. It was necessary to find the most appropriate rheological model. Test matrix for polymeric drilling fluid experiments are listed in Table 5.4.

Table 5.4 Test Matrix for Polymeric Drilling Fluid Experiments

	Minimum – Maximum
Average Liquid Flow Rate	25 – 110 gpm
Temperature	24 – 44°C

CHAPTER 6

RESULTS AND DISCUSSION

6.1 Water Experiments

Experiments with water were conducted to see the effect of temperature on the flow of Newtonian fluids in vertical concentric annulus. Calculations for friction pressure loss through annulus were performed by applying Newtonian model explained in Theory section with the effect of equivalent diameter concepts. (Bourgoyne Jr. et al., 1991) For this reason, for four different temperatures (20, 25, 35 and 45°C), friction pressure losses through annulus were estimated separately with equivalent diameter definitions of hydraulic radius (HR), slot flow approximation (SA), Lamb's (LC) and Crittendon's (CC) diameter.

Density and viscosity of water and diameter calculated with equivalent diameter concepts are listed below.

Table 6.1 Properties of Water (Bourgoyne Jr. et al., 1991)

Temperature (°C)	20	25	35	45
Density (ppg)	8.3304	8.3208	8.2956	8.2637
Viscosity (cp)	1.0005	0.8891	0.7198	0.5970

Table 6.2 Equivalent Diameter Values

Definition	Equivalent Diameter (in)
Hydraulic Radius (HR)	1.060
Slot Approximation (SA)	0.865
Lamb's Criteria (LC)	0.867
Crittendon Criteria (CC)	1.821

At 20°C, measured and calculated friction pressure losses are demonstrated in Table 6.3.

Table 6.3 Measured and Calculated Friction Pressure Loss for Water at 20°C

Measured Friction Pressure Loss (psi)	Flow Rate (gpm)	Calculated Friction Pressure Loss (psi) **(HR)**	Calculated Friction Pressure Loss (psi) **(SA)**	Calculated Friction Pressure Loss (psi) **(LC)**	Calculated Friction Pressure Loss (psi) **(CC)**
0.0273	40.6	0.020323	0.026205	0.026130	0.021548
0.03431	45.1	0.024428	0.031497	0.031407	0.025900
0.04125	50.5	0.029774	0.038390	0.038280	0.031568
0.04792	55.4	0.035012	0.045144	0.045015	0.037122
0.05754	60.6	0.040964	0.052819	0.052667	0.043432
0.06418	65.6	0.047060	0.060680	0.060505	0.049896
0.07348	70.7	0.053649	0.069174	0.068975	0.056881
0.09199	80.4	0.067185	0.086628	0.086379	0.071233
0.10251	85.5	0.074819	0.096472	0.096195	0.079328
0.11255	90.9	0.083284	0.107386	0.107077	0.088302
0.12627	96.7	0.092805	0.119662	0.119318	0.098397
0.14279	102.7	0.103115	0.132956	0.132574	0.109328
0.17354	112.3	0.120570	0.155462	0.155016	0.127835

Following graph (Figure 6.1) is given to represent these friction pressure loss vs. flow rate plot.

As it can be seen in Figure 6.1, measured friction pressure loss through annulus gave the results with the best agreement with slot approximation and Lamb's diameter. In order to investigate the effect of temperature, graph of measured pressure loss vs. Reynolds number calculated with slot approximation was examined at 20, 25, 35 and 45°C. It is demonstrated in Figure 6.2. Results for 25, 35 and 45°C are shown in Appendix.

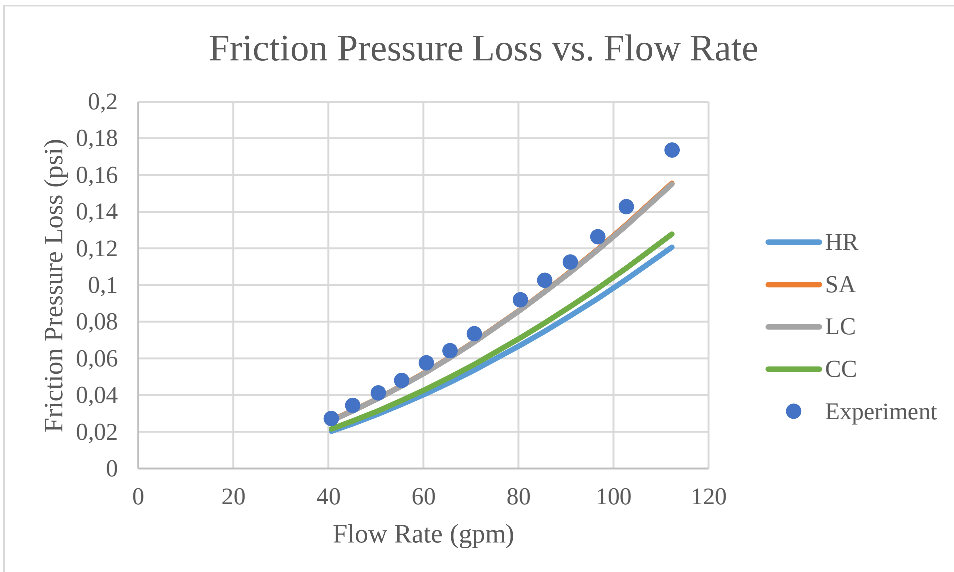

Figure 6.1 Friction Pressure Loss vs. Flow Rate at 20°C

As Reynolds number increased, the difference in friction pressure loss became more distinct with increasing temperature. This was related with viscosity and density terms in the formula of Reynolds number. The denominator of the Reynolds number formula decreased more significantly than the numerator with temperature and this caused the difference in friction pressure losses. Also, friction pressure loss increased with Reynolds number for all temperatures but this increase became more pronounced at lower temperature. Regime transition with temperature effect could not be examined due to critical flow rate for transition was very low to be achieved with this experimental setup.

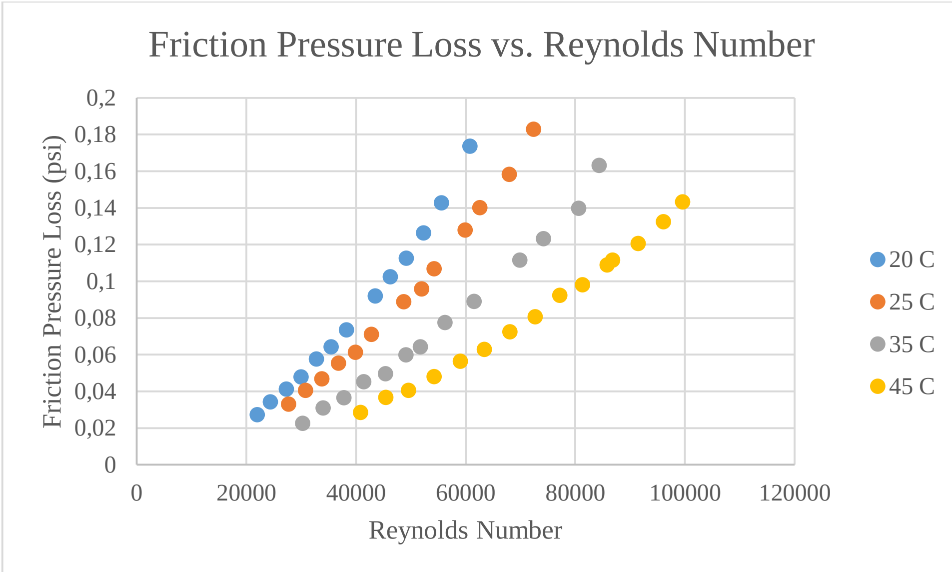

Figure 6.2 Friction Pressure Loss vs. Reynolds Number for Water

.

6.2 Polymeric Drilling Fluid Experiments

Experiments conducted by using polymeric drilling fluids were divided into two parts that were rheological measurements and friction pressure loss measurements. Results obtained from rheological measurements were used to find the most suitable rheological model for drilling fluids. Then, friction pressure losses through vertical concentric annular test section were determined with the selected model theoretically. All processes were repeated for all temperatures. Results from friction pressure loss experiments were used to compare with theoretical results to investigate the effect of temperature on the annular flow of polymeric drilling fluid.

6.2.1 Rheological Measurements

Rheological parameters for Bingham Plastic, Power Law and Herschel-Bulkley models were calculated by using dial readings at 600, 300, 200, 100, 6 and 3 rpm from viscometer during experiments with polymeric drilling fluid for different temperatures when reaching steady state.

Following table demonstrates all results obtained from viscometer measurements.

Table 6.4 Viscometer Dial Readings

Viscometer Speed (RPM)	Dial Reading 24°C	Dial Reading 30°C	Dial Reading 37°C	Dial Reading 44°C
600	27	24	21	18.5
300	19.5	17	16	13.5
200	16	15	13	11.5
100	12	11	10	8.5
6	4.5	4	3.5	3
3	3.5	3	3	2.5

As mentioned previously in Theory section of thesis, relationship between shear stress and shear rate should be examined to determine rheological parameters. After that, theoretically obtained shear stress values by using determined parameters were compared with measured ones for each model statistically and values of average error, standard deviation and coefficient of determination (R^2) were found with following formulas.

$$Error = \frac{\tau_{measured} - \tau_{calculated}}{\tau_{measured}} * 100 \tag{6.1}$$

$$Standard\ Deviation = \sqrt{\frac{|\tau_{calculated} - \overline{\tau_{calculated}}|^2}{5}} \tag{6.2}$$

At 24°C, firstly, Bingham Plastic model was investigated. For this reason, measured shear stress vs. shear rate graph shown in Figure 6.3 were plotted.

According to this graph, the slope of straight line and intersection point with x-axis gave plastic viscosity (μ_p) and yield point (τ_y), respectively. These values were used to determine shear stress theoretically. Table 6.5 and 6.6 shows results for Bingham Plastic model at 24°C.

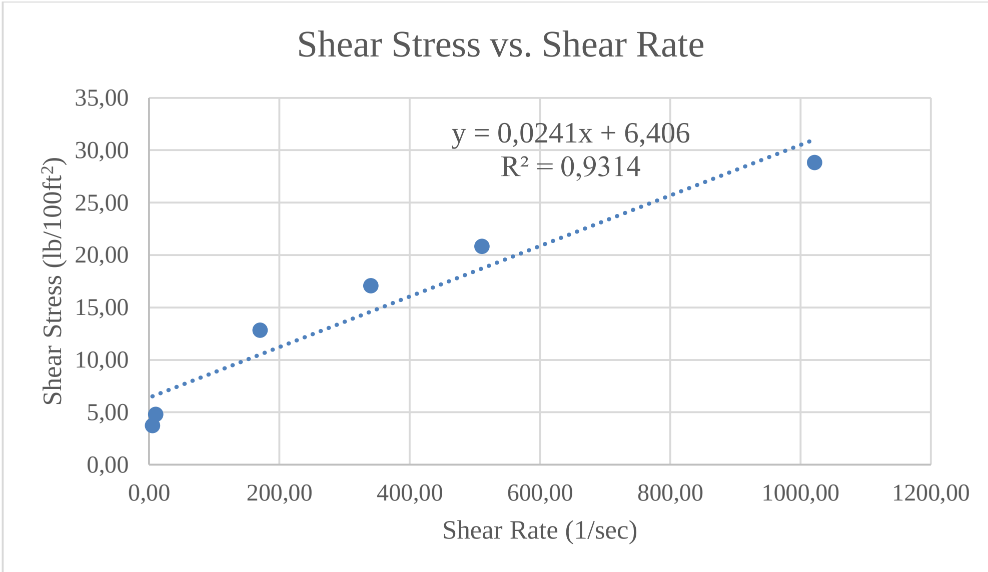

Figure 6.3 Measured Shear Stress vs. Shear Rate Graph at 24˚C

Table 6.5 Measured and Calculated Shear Stress Values for Bingham Plastic Model at 24˚C

Viscometer Speed (RPM)	Shear Rate (1/sec)	Dial Reading	Measured Shear Stress (lb/100ft^2)	Calculated Shear Stress (lb/100ft^2)	Error (%)
600	1021.80	27	28.83	31.05	7.70
300	510.90	19.5	20.82	18.73	10.06
200	340.60	16	17.08	14.62	14.42
100	170.30	12	12.81	10.51	17.95
6	10.22	4.5	4.81	6.65	38.44
3	5.11	3.5	3.74	6.53	74.70
				Av. Error	**27.21**
				St. Deviation	**9.30**
				R^2	**0.9314**

Table 6.6 Bingham Plastic Model Parameters at 24°C

μ_p (lb-s/100ft^2)	0.02
τ_y (lb/100ft^2)	6.41

Power Law model parameters at 24°C were determined by plotting the graph of logarithm of measured shear stress vs. logarithm of shear rate. (Figure 6.4)

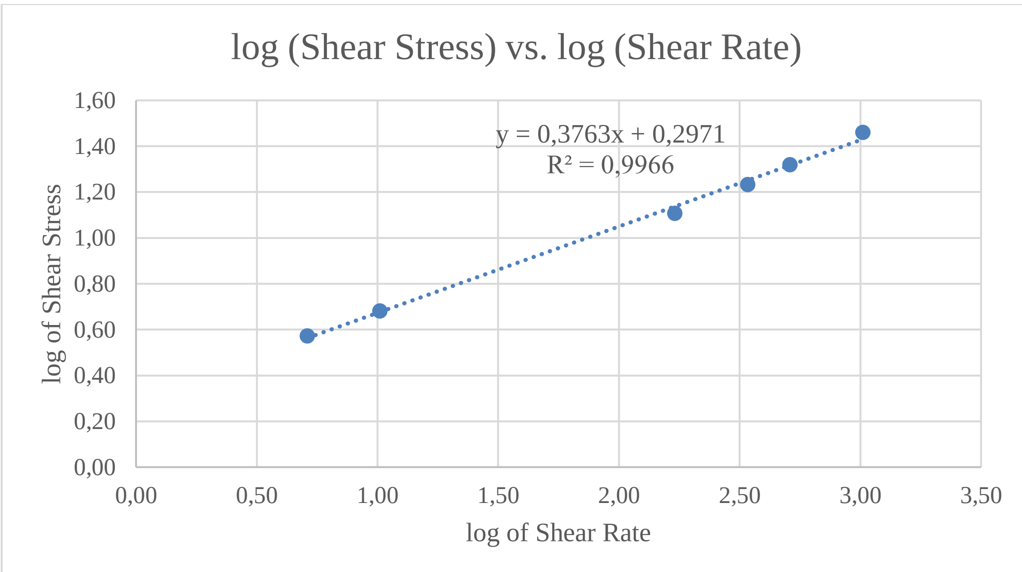

Figure 6.4 Log of Shear Stress vs. Log of Shear Rate Graph at 24°C

The slope of straight line obtained from graph gave flow behavior index (n_p) and intersection point with x-axis gave the logarithm of consistency index (K_p). Table 6.7 and 6.8 demonstrates results for Power Law rheological model at 24°C.

Table 6.7 Measured and Calculated Shear Stress Values for Power Law Model at 24°C

Viscometer Speed (RPM)	Shear Rate (1/sec)	Dial Reading	Measured Shear Stress (lb/100ft^2)	Calculated Shear Stress (lb/100ft^2)	Error (%)
600	1021.80	27	28.83	26.89	6.75
300	510.90	19.5	20.82	20.71	0.53
200	340.60	16	17.08	17.78	4.08
100	170.30	12	12.81	13.70	6.91
6	10.22	4.5	4.81	4.75	1.10
3	5.11	3.5	3.74	3.66	2.04
				Av. Error	**3.57**
				St. Deviation	**9.12**
				R^2	**0.9966**

Table 6.8 Power Law Model Parameters at 24°C

Flow Behavior Index (n_p)	0.38
Consistency Index (K_p) (lb-sec^n/100 ft^2)	1.98

Herschel-Bulkley model parameters at 24°C were found by using GRG Nonlinear Solving method in SOLVER add-in of Microsoft Excel because of the complexity of three parameters. In order to apply SOLVER function, initial values of parameters were determined by plotting the graph of logarithm of measured shear stress minus yield stress vs logarithm of shear rate. To plot this graph, firstly, yield point was found by Gucuyener's method. (Gucuyener, 1983) Then, like Power Law model, the slope of straight line obtained from graph gave the flow behavior index (n) and intersection point with x-axis gave the logarithm of consistency index (K). Following table shows the initial values of model parameters and figure shows the graph of logarithm of measured shear stress minus yield stress vs logarithm of shear rate.

Table 6.9 Initial Values of Herschel-Bulkley Parameters

Shear Rate (Geometric Mean) (γ_G) (1/sec)	72.25
Shear Stress at Geo. Mean of Shear Rate (τ_G) (lb/100ft^{2})	7.44
Yield Point (τ_y) (lb/100ft^2)	2.96
Flow Behavior Index (n)	0.64
Consistency Index (K) (lb-sec^n/100 ft^2)	0.34

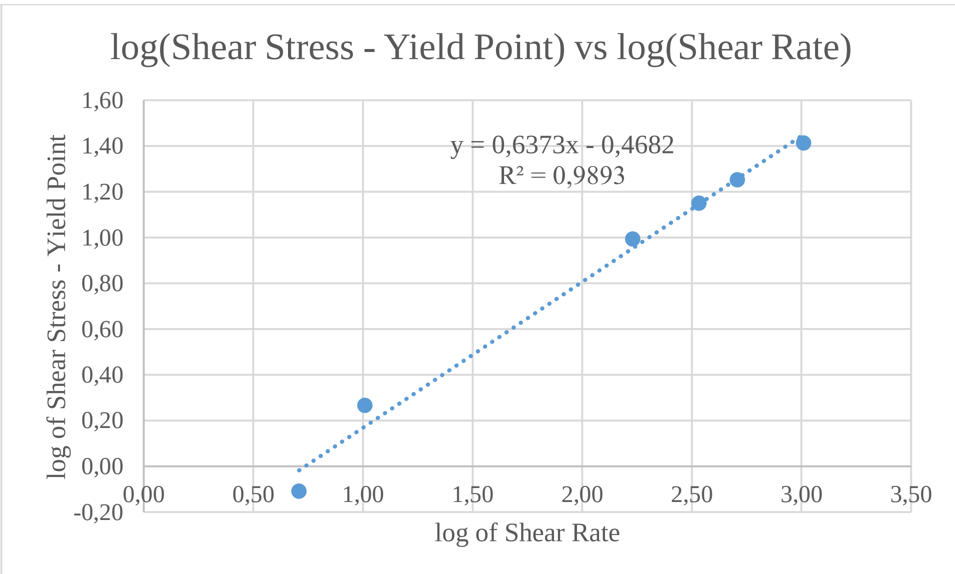

Figure 6.5 Log of Shear Stress vs. Log of Shear Rate Graph for Initial Parameters at 24°C

SOLVER found the optimum Herschel-Bulkley model parameters by minimizing the square of difference between calculated and measured shear stress values. According to results, table of measured and calculated shear stresses, the graph of logarithm of measured shear stress minus yield stress vs logarithm of shear rate and table of model parameters are shown below.

Table 6.10 Measured and Calculated Shear Stress Values for Herschel-Bulkley Model at $24^{\circ}C$

Viscometer Speed (RPM)	Shear Rate (1/sec)	Dial Reading	Measured Shear Stress ($lb/100ft^2$)	Calculated Shear Stress ($lb/100ft^2$)	Error (%)
600	1021.80	27	28.83	28.81	0.08
300	510.90	19.5	20.82	20.78	0.20
200	340.60	16	17.08	17.26	1.02
100	170.30	12	12.81	12.71	0.78
6	10.22	4.5	4.81	4.64	3.49
3	5.11	3.5	3.74	3.90	4.29
				Av. Error	**1.64**
				St. Deviation	**9.64**
				R^2	**0.998**

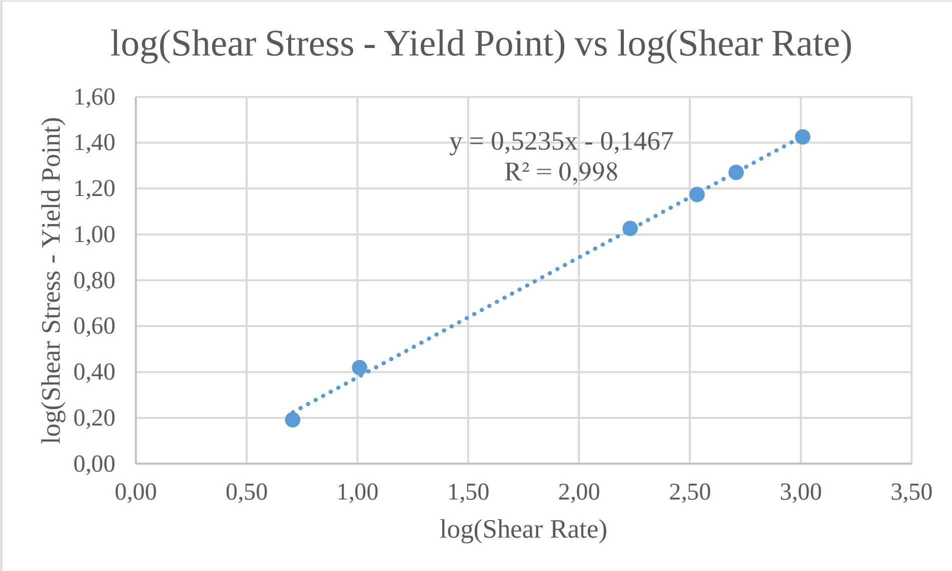

Figure 6.6 Log of Shear Stress vs. Log of Shear Rate Graph for SOLVER Parameters at 24°C

Table 6.11 Herschel-Bulkley Model Parameters at 24°C

Yield Point (τ_y)	2.18
Flow Behavior Index (n)	0.52
Consistency Index (K)	0.74

Procedures to determine rheological parameters and values of average error, standard deviation and coefficient of determination at 24°C were applied to other temperatures for each model. Following tables shows all results for 24, 30, 37 and 44 degrees Celsius.

Table 6.12 Model Parameters at 24°C

	Bingham Plastic Model	Power Law Model	Herschel-Bulkley Model
Average Error	27.21	3.57	1.64
Standard Deviation	9.30	9.12	9.64
R^2	0.9314	0.9966	0.9980
Plastic Viscosity (μ_p)	0.02		
Yield Point (τ_y)	6.41		2.18
Flow Behavior Index (n, n_p)		0.38	0.52
Consistency Index (K)		1.98	0.74

Table 6.13 Model Parameters at 30°C

	Bingham Plastic Model	Power Law Model	Herschel-Bulkley Model
Average Error	30.19	2.44	2.51
Standard Deviation	8.22	8.30	8.58
R^2	0.9175	0.9984	0.9979
Plastic Viscosity (μ_p)	0.02		
Yield Point (τ_y)	5.85		1.44
Flow Behavior Index (n, n_p)		0.38	0.48
Consistency Index (K)		1.72	0.89

Table 6.14 Model Parameters at 37°C

	Bingham Plastic Model	Power Law Model	Herschel-Bulkley Model
Average Error	29.86	3.96	1.61
Standard Deviation	7.20	7.29	7.55
R^2	0.9074	0.9969	0.9992
Plastic Viscosity (μ_p)	0.02		
Yield Point (τ_y)	5.43		1.18
Flow Behavior Index (n, n_p)		0.37	0.45
Consistency Index (K)		1.65	0.92

Table 6.15 Model Parameters at 44°C

	Bingham Plastic Model	Power Law Model	Herschel-Bulkley Model
Average Error	29.46	3.25	0.59
Standard Deviation	6.36	6.38	6.64
R^2	0.9176	0.9975	0.9999
Plastic Viscosity (μ_p)	0.02		
Yield Point (τ_y)	4.58		1.14
Flow Behavior Index (n, n_p)		0.38	0.47
Consistency Index (K)		1.38	0.69

In order to find the most suitable rheological model for polymeric drilling fluid at four different temperatures, all results were examined. As a result, based on average error and coefficient of correlation results, and for being consistent with API RP 13D manual, Herschel-Bulkley model gave more accurate prediction than other models. Then, friction pressure loss estimation was performed by using Herschel-Bulkley model.

6.2.2 Friction Pressure Loss Estimation

After choosing rheological model and determining rheological parameters, friction pressure losses were calculated with Herschel-Bulkley model. Friction pressure loss for concentric annular flow is estimated by considering equivalent diameter concepts mentioned in Theory section. In this study, friction pressure losses were estimated by applying different equivalent diameter concepts in Herschel-Bulkley model and the most suitable definition was chosen.

American Petroleum Institute Recommended Practice 13D for Rheology and Hydraulics of oil-well drilling fluids has represented the methodology for friction pressure loss estimation through annuli by applying Herschel-Bulkley rheological model. (American Petroleum Institute (API), 2009) As previously shown in Theory section, hydraulic radius concept has been used in calculation in API RP 13D. In this study, other equivalent diameter definitions named as slot flow approximation, Lamb's criteria and Crittendon's criteria were added to formulas instead of hydraulic radius, and friction pressure losses were calculated. The values of equivalent diameter for four different equivalent diameter concepts were shown in Table 6.2 previously.

Also, API RP 13D stated that Herschel-Bulkley model parameters were calculated with field measurements directly by using Equation 3.3, 3.4 and 3.5. However, in this study, in calculation of friction pressure loss, model parameters were obtained from SOLVER results. Since, average error value with parameters from field measurements was more than SOLVER results at 24^{o}C. (Table 6.16)

Table 6.16 Field Measurements-SOLVER Results Comparison at 24°C

	Field Measurements			SOLVER Results		
	Bingham Plastic Model	Power Law Model	Herschel-Bulkley Model	Bingham Plastic Model	Power Law Model	Herschel-Bulkley Model
Average Error	66.51	11.48	5.65	27.21	3.57	1.64
R^2	0.2949	0.8261	0.9834	0.9314	0.9966	0.9980
Standard Deviation	2.37	7.60	8.89	9.30	9.12	9.64

Rheological parameters used in estimation of friction pressure loss and densities of drilling fluid at 24, 30, 37 and 44ºC are listed in Table 6.17.

Table 6.17 Friction Pressure Loss Calculation Parameters

Temperature (°C)	24	30	37	44
Density (ppg)	8.323	8.309	8.29	8.267
Yield Point (τ_y) (lb/100 ft^2)	2.18	1.44	1.18	1.14
Flow Behavior Index (n)	0.52	0.48	0.45	0.47
Consistency Index (K) (lb-sec^n/100 ft^2)	0.74	0.89	0.92	0.69
Power Law Flow Behavior Index (n_p)	0.38	0.38	0.37	0.38

For 24°C, measured friction pressure loss and flow rate values are demonstrated below.

Table 6.18 Measured Friction Pressure Loss and Flow Rate Values at 24°C

P (psi)	Q (gpm)
0.0428	25.4
0.05554	30.4
0.05998	35.6
0.06717	40.5
0.07324	45.5
0.08024	50.4
0.08666	55.2
0.09865	60.8
0.11686	70.8
0.12041	75.5
0.12908	90.4
0.1378	95.5
0.16122	110.2

Despite all steps of calculation are shown in Theory, the procedure to find friction pressure loss is repeated. By using flow rates values, firstly, average velocity through annulus was calculated for all equivalent diameter concepts by using Equation 3.32 (Table 6.19).

Table 6.19 Average Velocities

Q (gpm)	Average Velocity (V_a) (ft/min)	
	HR, SA, LC	CC
25.4	123.39	187.77
30.4	147.67	224.73
35.6	172.93	263.17
40.5	196.74	299.39
45.5	221.03	336.36
50.4	244.83	372.58
55.2	268.14	408.06
60.8	295.35	449.46
70.8	343.93	523.38
75.5	366.76	558.13
90.4	439.14	668.28
95.5	463.91	705.98
110.2	535.32	814.65

Then, combined geometry shear rate correction factor (G) was calculated as 1.9659 (Eq. 3.34) and used in finding shear rates at wall (Eq. 3.35). By using Herschel-Bulkley model formula, shear stresses at wall were determined (Eq. 3.36). Shear stresses and shear rates at wall are shown in Table 6.20.

Table 6.20 Wall Shear Rates and Shear Stresses at 24°C

Q (gpm)	WALL SHEAR RATE (1/sec)				WALL SHEAR STRESS ($lb/100ft^2$)			
	γ_w (HR)	γ_w (SA)	γ_w (LC)	γ_w (CC)	τ_w (HR)	τ_w (SA)	τ_w (LC)	τ_w (CC)
25.4	366.14	448.70	447.67	324.36	19.55	21.41	21.38	18.54
30.4	438.21	537.03	535.79	388.21	21.18	23.21	23.19	20.07
35.6	513.17	628.89	627.44	454.62	22.74	24.95	24.92	21.53
40.5	583.80	715.45	713.80	517.19	24.11	26.47	26.44	22.82
45.5	655.88	803.77	801.92	581.04	25.43	27.94	27.91	24.06
50.4	726.51	890.33	888.28	643.62	26.66	29.30	29.27	25.21
55.2	795.70	975.13	972.88	704.91	27.80	30.57	30.54	26.29
60.8	876.43	1074.05	1071.58	776.43	29.08	31.99	31.96	27.49
70.8	1020.58	1250.71	1247.83	904.13	31.23	34.38	34.34	29.51
75.5	1088.33	1333.73	1330.66	964.15	32.19	35.45	35.41	30.41
90.4	1303.11	1596.95	1593.27	1154.43	35.06	38.63	38.59	33.10
95.5	1376.62	1687.04	1683.16	1219.55	35.99	39.66	39.62	33.97
110.2	1588.52	1946.72	1942.24	1407.28	38.53	42.49	42.44	36.37

After that, lower critical Reynolds number for laminar to transition flow regime and upper critical Reynolds number for transition to turbulent flow regime were found as 2761 and 3561, respectively (Eq. 3.38, 3.39), and generalized Reynolds numbers were calculated (Eq. 3.37) and then, friction factor values were estimated (Eq. 3.44) and tabulated in Table 6.21.

Table 6.21 Generalized Reynolds Number and Friction Factor at 24°C

Q (gpm)	GENERALIZED REYNOLDS NUMBER				FRICTION FACTOR			
	N_{ReG} (HR)	N_{ReG} (SA)	N_{ReG} (LC)	N_{ReG} (CC)	f (HR)	f (SA)	f (LC)	f (CC)
25.4	335	306	306	818	0.048	0.052	0.052	0.020
30.4	443	404	404	1082	0.036	0.040	0.040	0.015
35.6	565	515	516	1383	0.028	0.031	0.031	0.012
40.5	690	629	629	1689	0.023	0.025	0.025	0.009
45.5	826	752	753	2022	0.019	0.021	0.021	0.008
50.4	967	880	880	2367	0.017	0.018	0.018	0.007
55.2	1112	1011	1012	2723	0.014	0.016	0.016	0.006
60.8	1289	1172	1173	3159	0.012	0.014	0.014	0.006
70.8	1628	1479	1481	3991	0.010	0.011	0.011	0.005
75.5	1796	1631	1633	4404	0.009	0.010	0.010	0.005
90.4	2365	2146	2148	5800	0.007	0.007	0.007	0.005
95.5	2571	2333	2335	6307	0.006	0.007	0.007	0.005
110.2	3197	2899	2903	7846	0.006	0.006	0.006	0.004

Calculated friction pressure losses for four different equivalent diameter concept are listed in Table 6.22 (Eq. 3.45). Results of other temperatures are listed in Appendix.

Table 6.22 Calculated Friction Pressure Losses at 24°C

Q (gpm)	FRICTION PRESSURE LOSS (psi/ft)			
	dP_f/dL (HR)	dP_f/dL (SA)	dP_f/dL (LC)	dP_f/dL (CC)
25.4	0.0615	0.0825	0.0822	0.0339
30.4	0.0666	0.0894	0.0891	0.0367
35.6	0.0715	0.0961	0.0958	0.0394
40.5	0.0758	0.1020	0.1017	0.0418
45.5	0.0800	0.1076	0.1073	0.0440
50.4	0.0838	0.1129	0.1125	0.0462
55.2	0.0874	0.1178	0.1174	0.0493
60.8	0.0914	0.1233	0.1229	0.0564
70.8	0.0982	0.1325	0.1320	0.0718
75.5	0.1012	0.1366	0.1361	0.0793
90.4	0.1104	0.1489	0.1484	0.1043
95.5	0.1142	0.1530	0.1525	0.1135
110.2	0.1371	0.1730	0.1725	0.1412

Graphical representation of measured and estimated friction pressure losses for 24, 30, 37 and 44°C are demonstrated in Figure 6.7, 6.8, 6.9, 6.10.

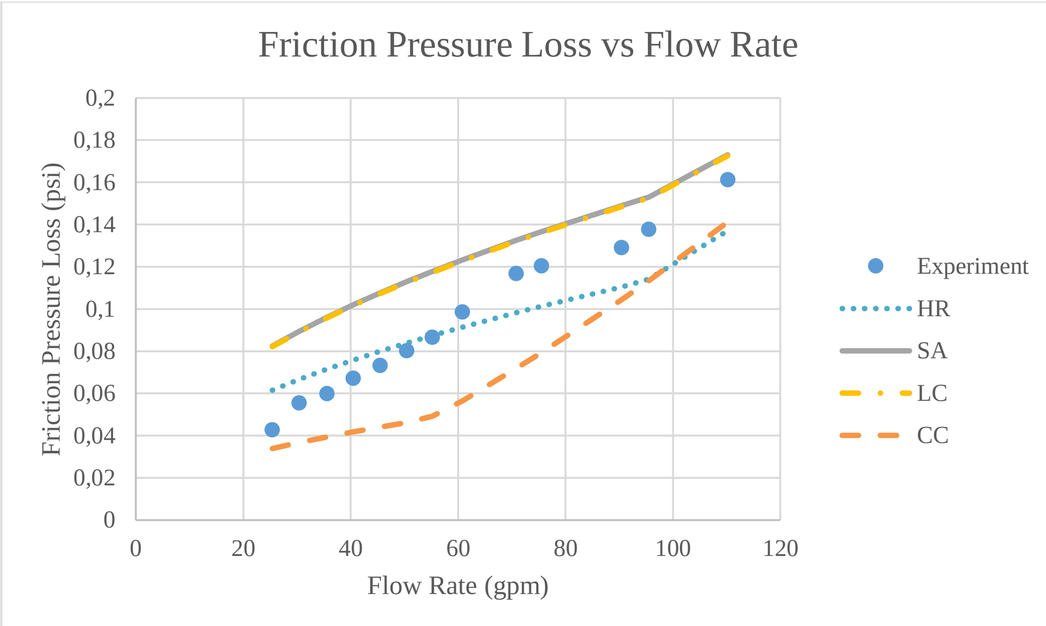

Figure 6.7 Measured and Calculated Friction Pressure Loss vs. Flow Rate at 24°C

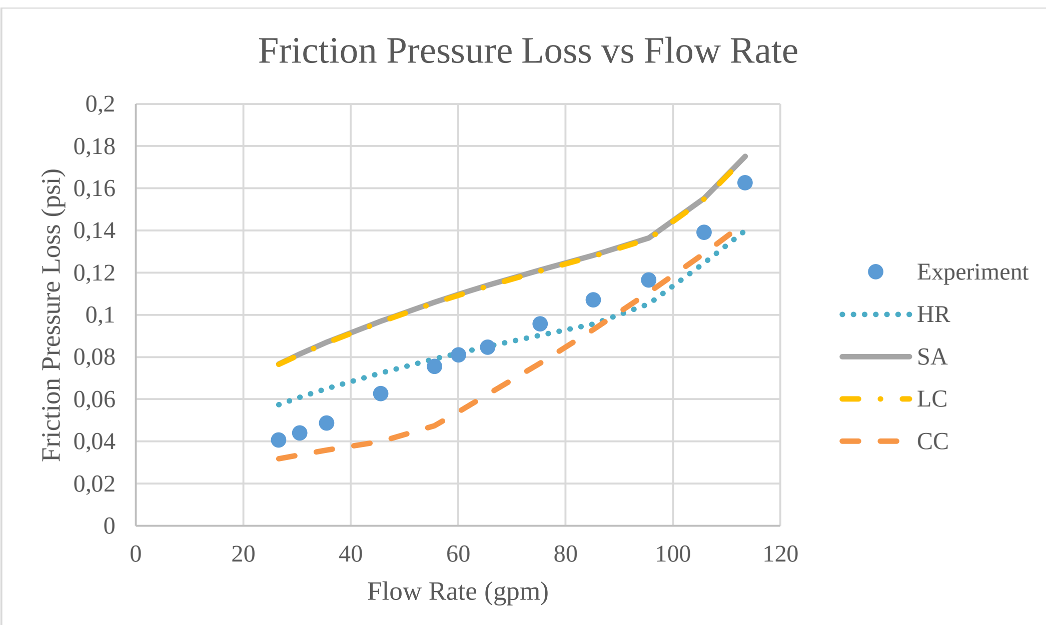

Figure 6.8 Measured and Calculated Friction Pressure Loss vs. Flow Rate at 30°C

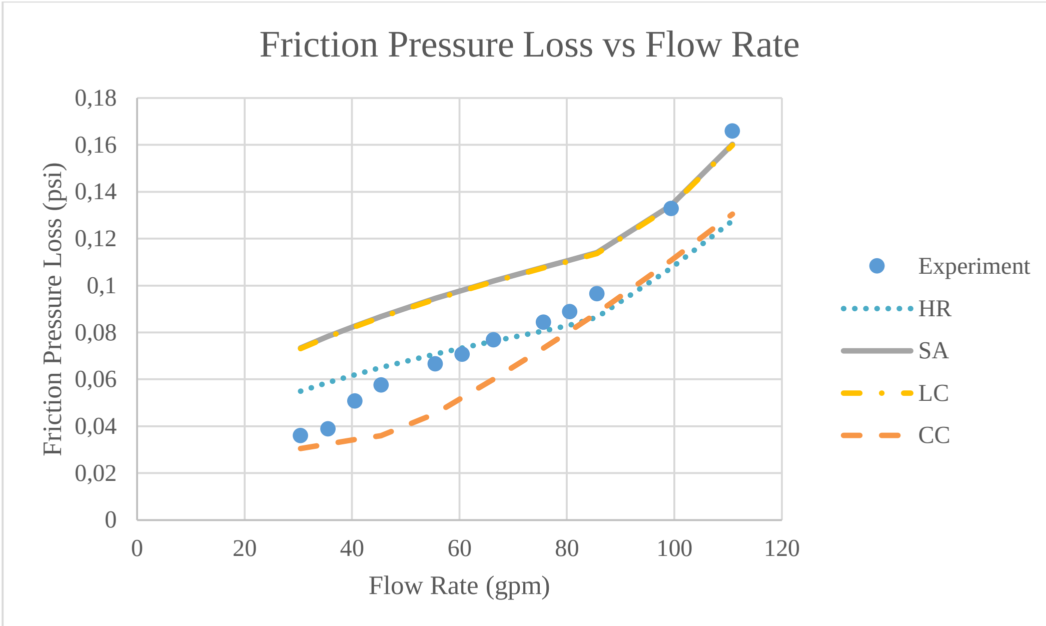

Figure 6.9 Measured and Calculated Friction Pressure Loss vs. Flow Rate at 37°C

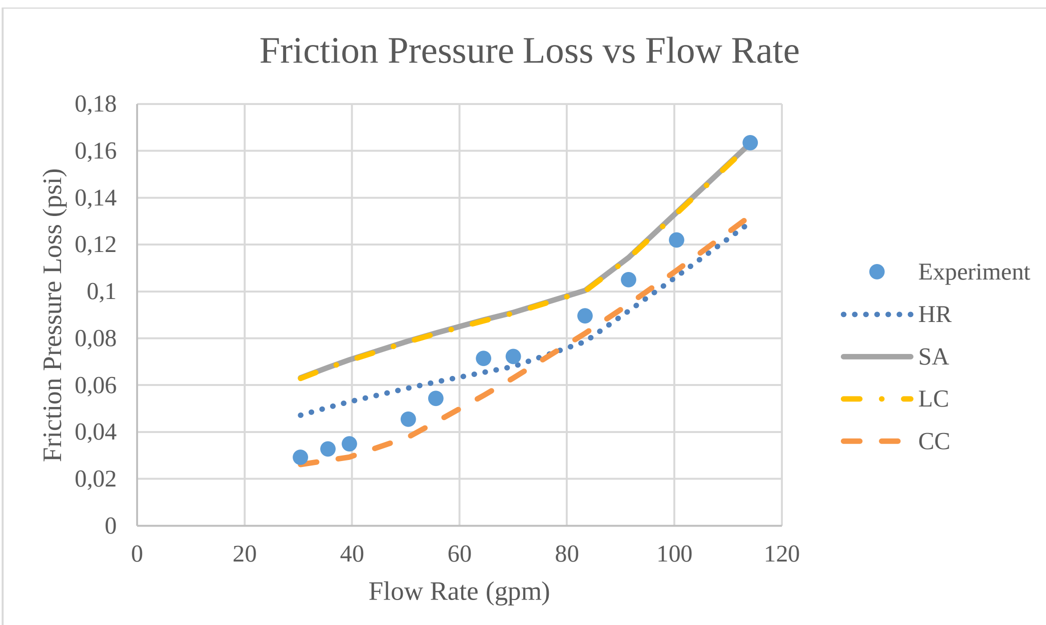

Figure 6.10 Measured and Calculated Friction Pressure Loss vs. Flow Rate at 44°C

When examining the graphs of friction pressure loss vs. flow rate, for all temperatures, it was observed that friction pressure loss calculated by applying hydraulic radius concept gave good agreement. It was expected because API RP 13D has used this definition.

However, after a certain point it was observed that slot approximation or Lamb's criteria matched better than the hydraulic radius concept. By using lower and upper critical Reynolds number, for all temperature values, flow regimes were determined to find out the reason of these deviation. Then, it was observed that transition from laminar flow regime caused the deviation, and graphs plotted by using hydraulic radius in laminar flow regime, slot approximation after end of laminar flow regime are represented below for all temperature values.

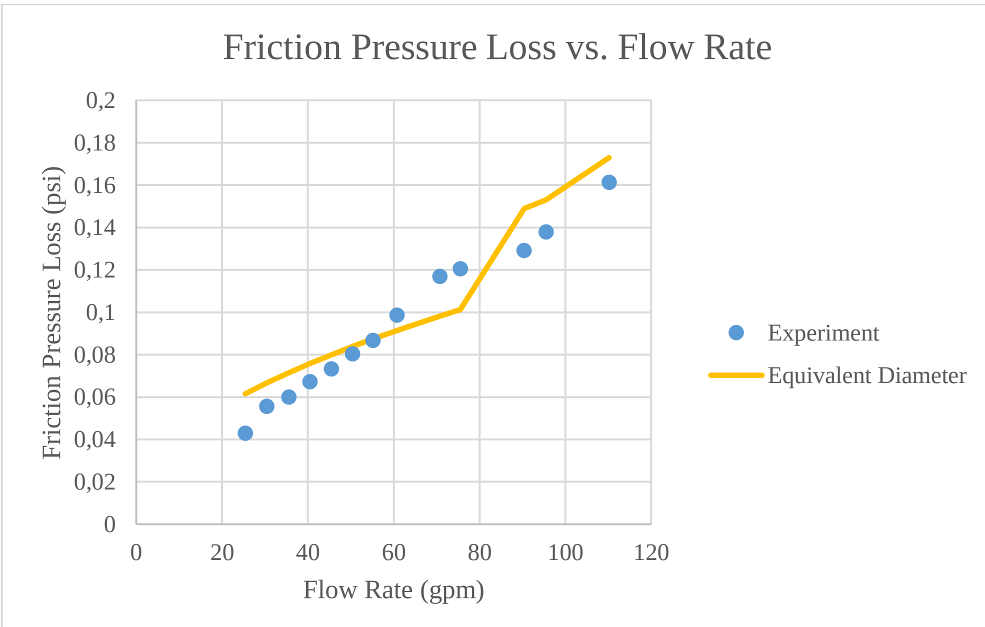

Figure 6.11 Friction Pressure Loss vs. Flow Rate at 24°C

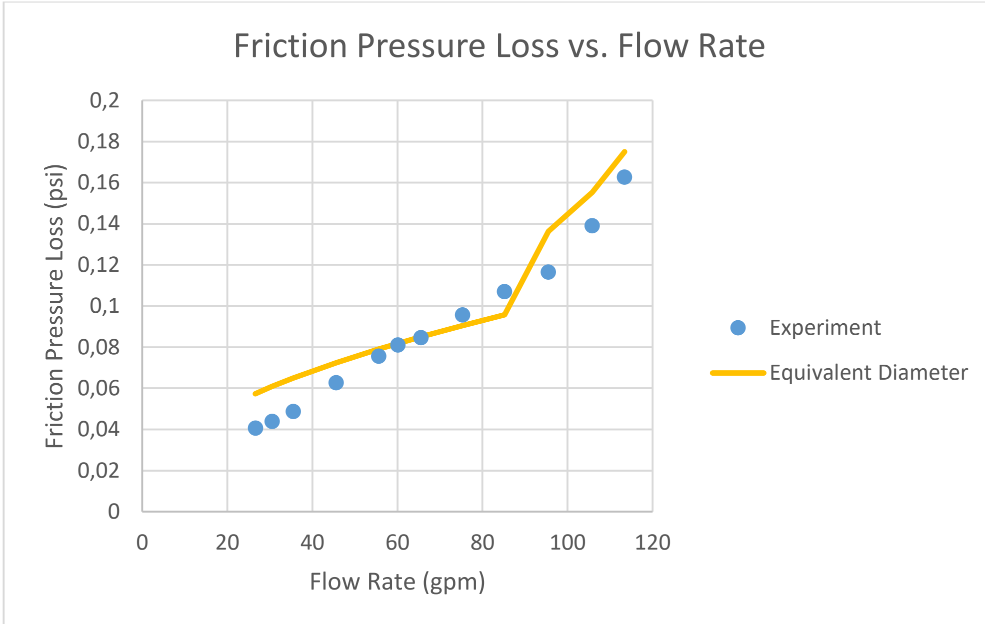

Figure 6.12 Friction Pressure Loss vs. Flow Rate at 30˚C

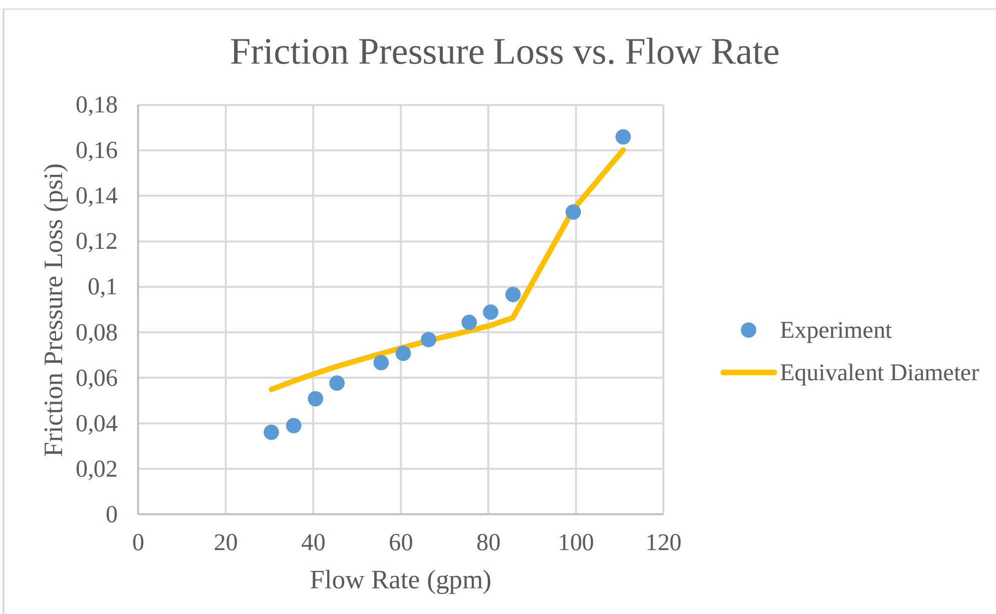

Figure 6.13 Friction Pressure Loss vs. Flow Rate at 37˚C

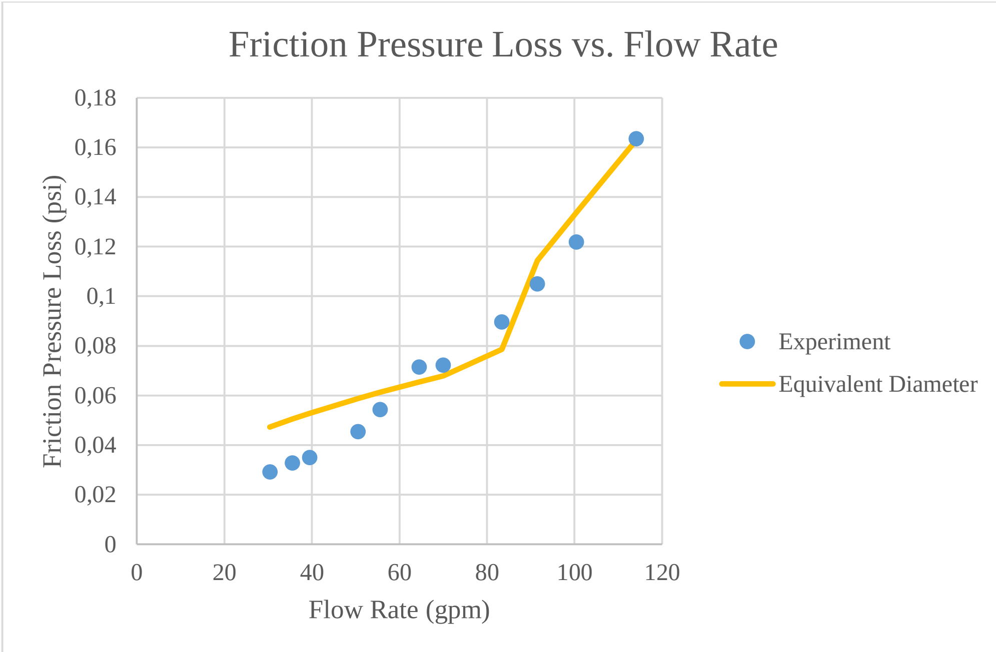

Figure 6.14 Friction Pressure Loss vs. Flow Rate at 44°C

6.3 Investigation of Temperature Effect

In order to examine temperature effect on friction pressure loss through the annulus, the components of the friction pressure loss calculation were investigated. For this reason, Relationships of Herschel-Bulkley parameters (yield point, flow behavior index and consistency index), apparent viscosity and Reynolds number with temperature were plotted and interpreted, respectively.

Following table represents Herschel-Bulkley model parameters for four different temperature values.

Table 6.23 Herschel-Bulkley Model Parameters

	Temperature (°C)			
	24	30	37	44
Yield Point (τ_y) (lb/100ft^2)	2.18	1.44	1.18	1.14
Flow Behavior Index (n)	0.52	0.48	0.45	0.47
Consistency Index (K) (lb-sec^n/100 ft^2)	0.74	0.89	0.92	0.69

Figure 6.15, 6.16 and 6.17 shows the plot of these parameters vs. temperature. According to these graphs, it was observed that temperature did not affect flow behavior index significantly, but consistency index initially increased and then decreased with increasing temperature distinguishably. Normally, it is expected to decrease in value of consistency index since it represents the viscosity of the fluid at low shear rates. (MI Swaco, 1998) Therefore, it could not be sufficient to understand the effect of temperature. Study of Romagnoli about temperature effect on rheology of drilling fluid have shown the similar results for flow behavior index and consistency index of Herschel-Bulkley model. (Romagnoli, 2017) It strengthened the idea of the complex effect of temperature on rheological parameters of drilling fluids. It could also be stated about flow behavior index

and consistency index graphs that changes in the trends of lines with temperature were inversely proportional as expected. Also, yield point decreased with increasing temperature. This represented the effect of temperature properly.

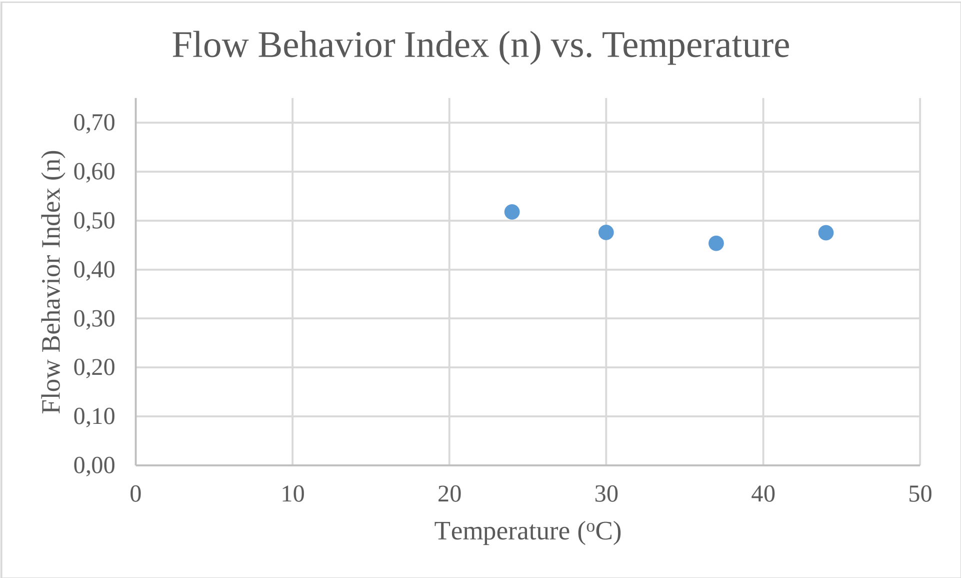

Figure 6.15 Flow Behavior Index vs. Temperature for Herschel-Bulkley Model

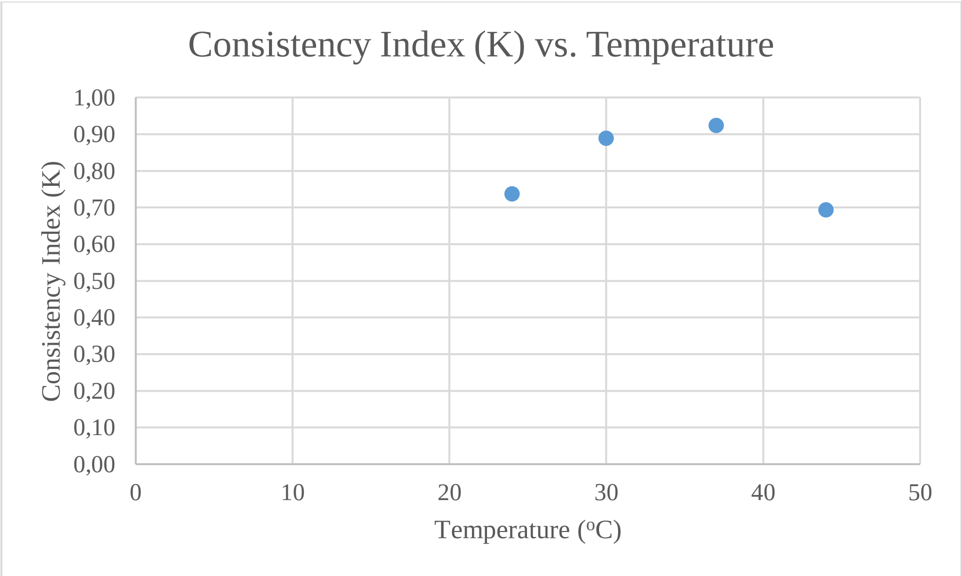

Figure 6.16 Consistency Index vs. Temperature for Herschel-Bulkley Model

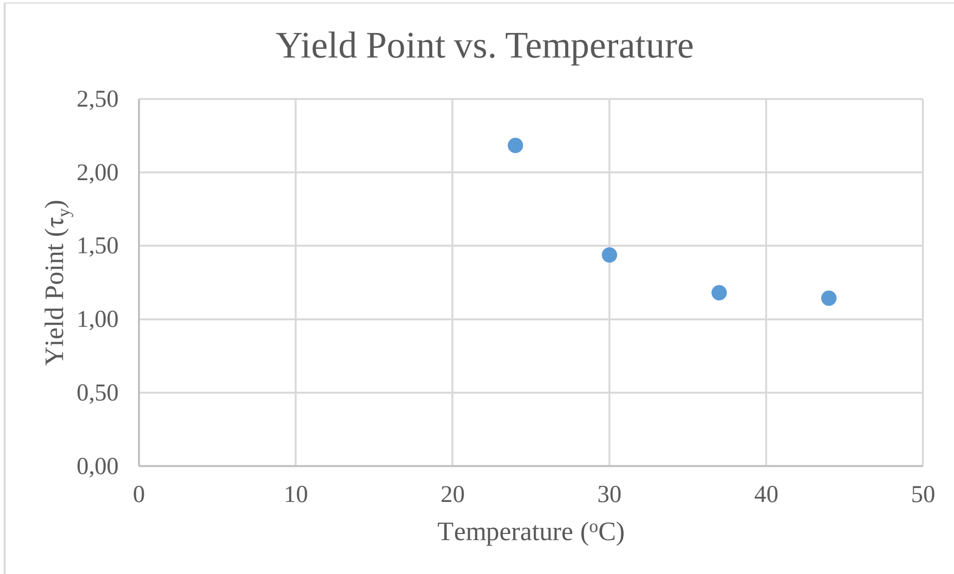

Figure 6.17 Yield Point vs. Temperature for Herschel-Bulkley Model

In order to see the combined behavior of these parameters, temperature effect of apparent viscosity was examined. According to comparison of measured and calculated friction pressure losses in above section, it was observed that in laminar flow regime, hydraulic radius, when flow regime started to change to transition, slot approximation showed good agreement. Therefore, in calculation of apparent viscosity, these two equivalent diameter definitions were applied together for different flow regimes. Apparent viscosity was calculated for varying flow rates from 25 to 125 gpm in order to observe the combined effect of temperature and flow rate. Following graph shows this relationship.

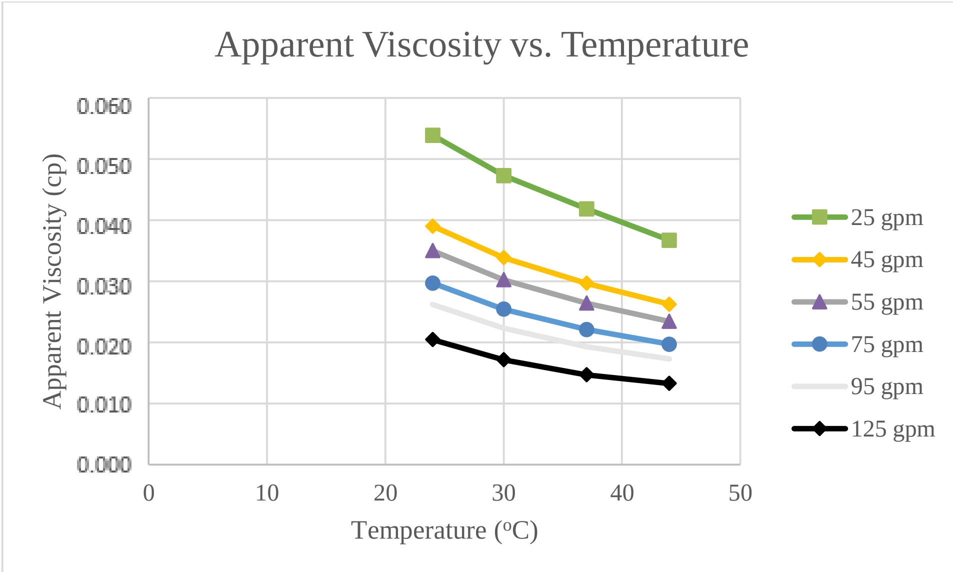

Figure 6.18 Apparent Viscosity vs. Temperature Graph

Apparent viscosity changed with temperature inversely as expected and high viscosity was influenced by temperature much more than low viscosity. In addition to effect of temperature, decrease in apparent viscosity had also inverse relationship with increasing flow rate due to shear thinning behavior of our polymeric drilling fluid.

Like apparent viscosity, generalized Reynolds number was calculated by considering different equivalent diameter concepts for flow regimes. It was also calculated at different flow rates for temperature values of 24, 30, 37 and 44°C. Figure 6.20 demonstrates the graph of generalized Reynolds number vs. temperature.

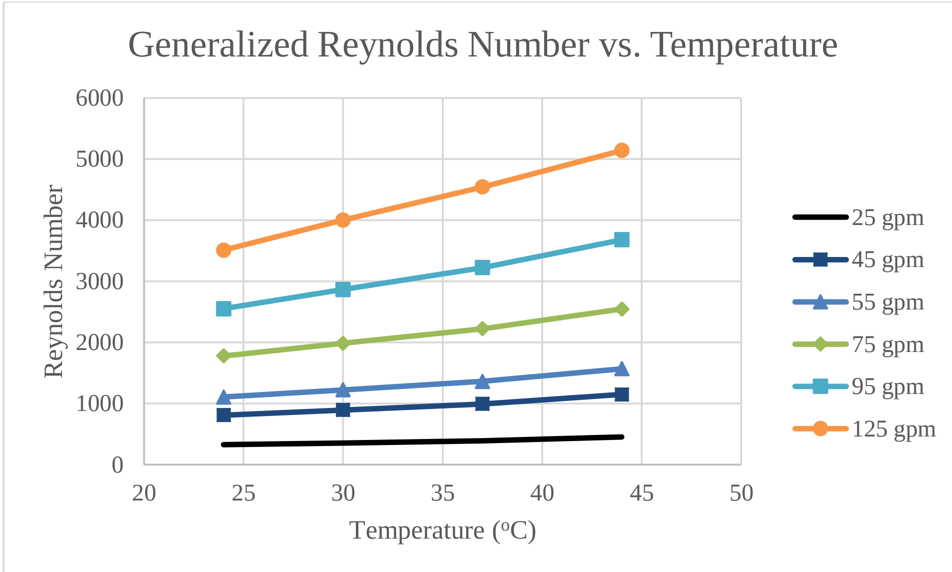

Figure 6.19 Generalized Reynolds Number vs. Temperature Graph

Generalized Reynolds number graph showed that when flow rate or shear rate increased, the effect of temperature on generalized Reynolds number became more pronounced. This was because of the change in density and apparent viscosity that were temperature dependent parameters used in calculation of this number. Density shown in Table 6.17 decreased with increasing temperature less significantly than decrease in viscosity. Therefore, Reynolds number increased with increasing temperature and this caused earlier regime transition.

The effect of temperature on friction pressure loss was investigated by plotting measured friction pressure loss vs. Reynolds number graph shown in Figure 6.19.

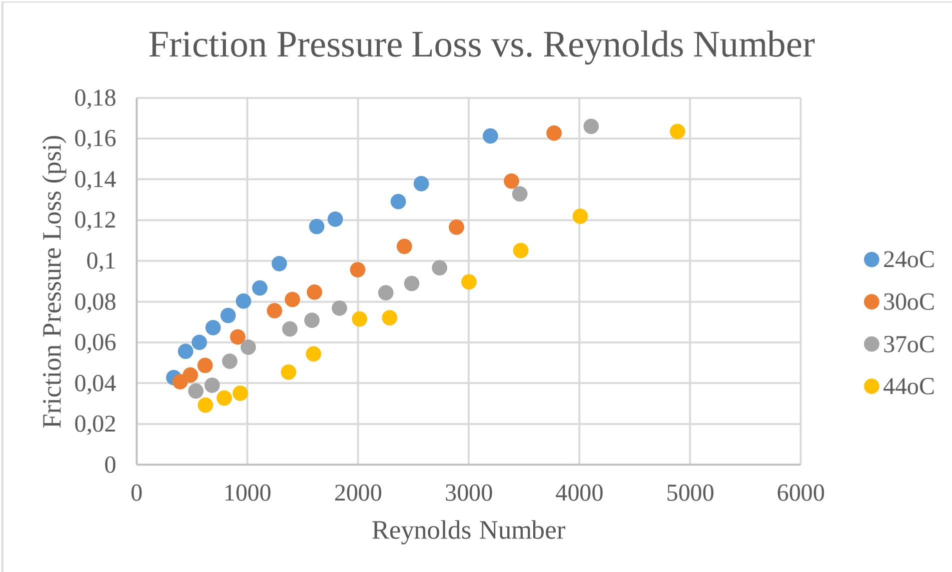

Figure 6.20 Friction Pressure Loss vs. Reynolds Number for Polymeric Drilling Fluid

This graph showed that friction pressure loss decreased with increasing temperature. It also demonstrated the total effect of all temperature dependent parameters.

CHAPTER 7

CONCLUSIONS

This study investigated the effect of temperature on friction pressure loss of polymeric drilling fluid prepared by using polyanionic cellulose and xanthan gum through vertical concentric annulus experimentally.

Following conclusions are drawn by comparing experimental works with theoretical information.

1. In water experiments, friction pressure loss vs. flow rate plots matched perfectly with theoretical results obtained by using Newtonian model with equivalent diameter definition of slot flow approximation. Also, change in Reynolds number with friction pressure loss became more pronounced at lower temperature.
2. Slot flow approximation gave the same results with Lamb's diameter as equivalent diameter definitions in calculation of friction pressure loss for water and polymeric drilling fluid.
3. When rheological measurements for six different viscometer speeds were examined, it was observed that Herschel-Bulkley rheological model gave the best description of our polymeric drilling fluid compared to Bingham Plastic and Power Law models in the range of test temperatures in terms of average error and coefficient of determination.

4. In the calculation of friction pressure loss by using Herschel-Bulkley model, parameters obtained from SOLVER was used because SOLVER results gave less average error than field measurements used in API RP 13D.
5. According to polymeric drilling fluid experiment results, in laminar flow regime, hydraulic radius agreed with experiments, after transition from laminar flow regime, slot flow approximation and Lamb's diameter gave more accurate results than other equivalent diameter definitions.
6. Consistency index and yield point of polymeric fluid were more sensitive to change in temperature than flow behavior index. Also, consistency index and flow behavior index showed complex behavior with increasing temperature.
7. Apparent viscosity of polymeric drilling fluid reflecting overall effects of Herschel-Bulkley model parameters showed exponential decrease with increasing temperature. It was more pronounced in low shear rates due to combined effect of temperature and shear thinning behavior.
8. Reynolds number vs. temperature graph for different flow rates showed that when flow rate or shear rate increases, the difference in Reynolds became more significant than low shear rates. This indicated that transition of laminar flow regime to turbulent flow became earlier with increasing temperature.
9. Friction pressure loss decreased with increasing temperature when examining measured friction loss vs. Reynolds number plot.

CHAPTER 8

RECOMMENDATIONS

This study examined the effect of temperature on friction pressure loss of polymeric drilling fluid through vertical concentric annulus experimentally. Because of the importance of friction pressure loss in drilling operations, experiments should be performed by simulating real drilling conditions including the effect of eccentricity, inclination, pipe rotation, annular geometry, and additive concentrations in addition to the effect of temperature. Also, the combined effect of these parameters should be modeled for accurate estimation of friction pressure loss.

Friction pressure loss estimation was conducted by using the method presented by American Petroleum Institute Recommended Practice 13D for rheology and hydraulics of oil-well drilling fluids. However, field measurements were not used to find the rheological parameters of Herschel-Bulkley model as stated in this manual due to the inaccuracy of low shear rate readings obtained visually from viscometer. Therefore, viscometer should measure and save the dial readings automatically.

REFERENCES

Ahmed, R. (2005). Experimental Study and Modeling of Yield Power-Law Fluid Flow in Pipes and Annuli. Tulsa, Oklahoma.

Ahmed, R. M., Enfis, M. S., El Kheir, H. M., Laget, M., & Saasen, A. (2010). The Effect of Drillstring Rotation on Equivalent Circulation Density: Modeling and Analysis of Field Measurements. In SPE Annual Technical Conference and Exhibition. Florence, Italy: Society of Petroleum Engineers. https://doi.org/10.2118/135587-MS

American Petroleum Institute (API). (2009). API Recommended Practice 13D – Rheology and hydraulics of oil-well drilling fluids.

Anifowoshe, O. L., & Osisanya, S. O. (2012). The Effect of Equivalent Diameter Definitions on Frictional Pressure Loss Estimation in an Annulus with Pipe Rotation. In SPE Deepwater Drilling and Completions Conference. Galveston, Texas: Society of Petroleum Engineers. https://doi.org/10.2118/151176-MS

Bourgoyne Jr., A. T., Millhelm, K. K., Chenevert, M. E., & Young Jr., F. S. (1991). Applied Drilling Engineering. (J. F. Evers & D. S. Pye, Eds.), Spe Textbook Series (Second Pri, Vol. 2). Richardson, TX: Society of Petroleum Engineers.

Chen, N. H. (1979). An Explicit Equation for Friction Factor in Pipe. Industrial & Engineering Chemistry Fundamentals, 18(3), 296–297. https://doi.org/10.1021/i160071a019

Chhabra, R. P., & Richardson, J. F. (2008). Non-Newtonian fluid behaviour. In Non-Newtonian Flow and Applied Rheology (2nd Editio, pp. 1–55). Butterworth-Heinemann. https://doi.org/10.1016/B978-0-7506-8532-0.00002-0

Colebrook, C. F. (1939). Turbulent Flow in Pipes, with Particular Reference to the Transition between the Smooth and Rough Pipe Laws. Journal of the Institution of Civil Engineers, 11(4), 133–156. https://doi.org/10.1680/ijoti.1939.13150

Crittendon, B. C. (1959). The Mechanics of Design and Interpretation of Hydraulic Fracture Treatments. Journal of Petroleum Technology, 11(10), 21–29. https://doi.org/10.2118/1106-G

Demirdal, B., & Cunha, J. C. S. (2007). Pressure Losses Of Non-Newtonian Fluids In Drilling Operations. In International Oil Conference and Exhibition in Mexico.

Vericruz, Mexico: Society of Petroleum Engineers. https://doi.org/10.2118/108711-MS

Dodge, D. W., & Metzner, A. B. (1959). Turbulent flow of non-newtonian systems. AIChE Journal, 5(2), 189–204. https://doi.org/10.1002/aic.690050214

Dosunmu, I. T., & Shah, S. N. (2015). Friction Pressure Prediction for Annular Flow of Power Law Fluids. Chemical Engineering Communications, 202(10), 1380–1388. https://doi.org/10.1080/00986445.2014.938806

Enfis, M. S., Ahmed, R. M., & Saasen, A. (2011). The Hydraulic Effect of Tool-joint on Annular Pressure Loss. In SPE Production and Operations Symposium. Oklahoma City, OK: Society of Petroleum Engineers. https://doi.org/10.2118/142282-MS

Fredrickson, A., & Bird, R. B. (1958). Non-Newtonian Flow in Annuli. Industrial & Engineering Chemistry, 50(3), 347–352. https://doi.org/10.1021/ie50579a035

Gucuyener, I. H. (1983). A Rheological Model for Drilling Fluids and Cement Slurries. In Middle East Oil Technical Conference and Exhibition (Vol. 3, pp. 389–393). Manama, Bahrain: Society of Petroleum Engineers. https://doi.org/10.2118/11487-MS

Gücüyener, I. H., & Mehmetoglu, T. (1992). Flow of yield-pseudo-plastic fluids through a concentric annulus. AIChE Journal, 38(7), 1139–1143. https://doi.org/10.1002/aic.690380717

Gücüyener, I. H., & Mehmetoğlu, T. (1996). Characterization of flow regime in concentric annuli and pipes for yield-pseudoplastic fluids. Journal of Petroleum Science and Engineering, 16(1–3), 45–60. https://doi.org/10.1016/0920-4105(96)00025-3

Haciislamoglu, M., & Langlinais, J. (1990). Non-Newtonian Flow in Eccentric Annuli. Journal of Energy Resources Technology, 112(3), 163. https://doi.org/10.1115/1.2905753

Hanks, R. W. (1963). The laminar-turbulent transition for flow in pipes, concentric annuli, and parallel plates. AIChE Journal, 9(1), 45–48. https://doi.org/10.1002/aic.690090110

Jensen, T. B., & Sharma, M. P. (1987). Study of Friction Factor and Equivalent Diameter Correlations for Annular Flow of Non-Newtonian Drilling Fluids. Journal of Energy Resources Technology, 109(4), 200. https://doi.org/10.1115/1.3231347

Kelessidis, V. C., Maglione, R., Tsamantaki, C., & Aspirtakis, Y. (2006). Optimal determination of rheological parameters for Herschel–Bulkley drilling fluids and impact on pressure drop, velocity profiles and penetration rates during drilling.

Journal of Petroleum Science and Engineering, 53(3–4), 203–224. https://doi.org/10.1016/j.petrol.2006.06.004

Lamb, H. (1945). Hydrodynamics (6th Ed).

Meter, D. M., & Byron Bird, R. (1961). Turbulent newtonian flow in annuli. AIChE Journal, 7(1), 41–45. https://doi.org/10.1002/aic.690070112

Metzner, A. B., & Reed, J. C. (1955). Flow of non-newtonian fluids—correlation of the laminar, transition, and turbulent-flow regions. AIChE Journal, 1(4), 434–440. https://doi.org/10.1002/aic.690010409

MI Swaco. (1998). Rheology and Hydraulics. In MI Swaco - Drilling Fluids Handbook (p. 5.1-5.36). MI Swaco.

Okafor, M. N., & Evers, J. F. (1992). Experimental Comparison of Rheology Models for Drilling Fluids. In SPE Western Regional Meeting (pp. 575–581). Bakersfield, California: Society of Petroleum Engineers. https://doi.org/10.2118/24086-MS

Ozbayoglu, E. M., & Sorgun, M. (2010). Frictional Pressure Loss Estimation of Non-Newtonian Fluids in Realistic Annulus With Pipe Rotation. Journal of Canadian Petroleum Technology, 49(12), 57–64. https://doi.org/10.2118/141518-PA

Rabia, H. (2001). Practical Rig Hydraulics. In Well Engineering & Construction (pp. 303–336).

Reed, T. D., & Pilehvari, A. A. (1993). A New Model for Laminar, Transitional, and Turbulent Flow of Drilling Muds. In SPE Production Operations Symposium (pp. 469–482). Oklahoma City, OK. https://doi.org/10.2118/25456-MS

Romagnoli, R. (2017). New Achievements Concerning Temperature Effects on Mud Rheology and Hydraulic Performance While Drilling (pp. 1–11). Retrieved from https://www.onepetro.org/download/conference-paper/OMC-2017-551?id=conference-paper%2FOMC-2017-551

Rooki, R. (2015). Estimation of Pressure Loss of Herschel–Bulkley Drilling Fluids During Horizontal Annulus Using Artificial Neural Network. Journal of Dispersion Science and Technology, 36(2), 161–169. https://doi.org/10.1080/01932691.2014.904793

Schuh, F. J. (1965). Computer makes surge-pressure calculation useful. Oil and Gas Journal, 96–104.

Sorgun, M., & Ozbayoglu, M. E. (2010). A mechanistic model for predicting frictional pressure losses for newtonian fluids in concentric annulus. Petroleum Science and Technology, 28(16), 1665–1673. https://doi.org/10.1080/10916460903226064

Sorgun, M., & Ozbayoglu, M. E. (2011). Predicting Frictional Pressure Loss During Horizontal Drilling for Non-Newtonian Fluids. Energy Sources, Part A: Recovery, Utilization, and Environmental Effects, 33(7), 631–640. https://doi.org/10.1080/15567030903226264

Subramanian, R., & Azar, J. J. (2000). Experimental Study on Friction Pressure Drop for NonNewtonian Drilling Fluids in Pipe and Annular Flow. In International Oil and Gas Conference and Exhibition in China. Beijing, China: Society of Petroleum Engineers. https://doi.org/10.2118/64647-MS

Ulker, E., Sorgun, M., Solmus, I., & Karadeniz, Z. H. (2017). Determination of Newtonian Fluid Flow Behavior Including Temperature Effects in Fully Eccentric Annulus. Journal of Energy Resources Technology, 139(4), 042001-1–5. https://doi.org/10.1115/1.4035908

Zamora, M., Roy, S., & Slater, K. (2005). Comparing a Basic Set of Drilling Fluid Pressure-Loss Relationships to Flow-Loop and Field Data. AADE National Technical Conference and Exhibition. Retrieved from http://scholar.google.no/scholar?cluster=14681169229685361298&hl=no&as_sdt=2005&sciodt=0,5

APPENDIX

Water Experiments

Table A 1 Measured Friction Pressure Loss at 25°C

Measured Friction Pressure Loss (psi)	Flow Rate (gpm)
0.03299	45.6
0.04055	50.6
0.04678	55.5
0.05537	60.5
0.0613	65.6
0.07108	70.4
0.08889	80.1
0.09576	85.5
0.10683	89.2
0.12797	98.5
0.14019	102.9
0.15818	111.7
0.18283	119

Table A 2 Measured Friction Pressure Loss at 35°C

Measured Friction Pressure Loss (psi)	**Flow Rate (gpm)**
0.02253	40.4
0.03084	45.4
0.03658	50.5
0.04521	55.3
0.04964	60.6
0.05982	65.6
0.06423	69.1
0.07748	75.1
0.08897	82.2
0.11151	93.3
0.12325	99.1
0.13968	107.6
0.16314	112.6

Table A 3 Measured Friction Pressure Loss at 45°C

Measured Friction Pressure Loss (psi)	Flow Rate (gpm)
0.02839	45.4
0.03669	50.5
0.04049	55.1
0.04794	60.3
0.05644	65.6
0.0629	70.5
0.07237	75.7
0.08064	80.8
0.0923	85.8
0.09813	90.4
0.10895	95.4
0.11159	96.5
0.12051	101.7
0.13249	106.8
0.14333	110.7

Polymeric Drilling Fluid Experiments

Table A 4 Measured Friction Pressure Loss at 30°C

Measured Friction Pressure Loss (psi)	**Flow Rate (gpm)**
0.04065	26.6
0.04395	30.5
0.04864	35.5
0.06262	45.6
0.07555	55.6
0.081	60.1
0.08462	65.5
0.0957	75.3
0.10708	85.2
0.11656	95.5
0.13908	105.8
0.16263	113.43

Table A 5 Measured Friction Pressure Loss at 37°C

Measured Friction Pressure Loss (psi)	Flow Rate (gpm)
0.0361	30.4
0.03892	35.5
0.05081	40.5
0.05763	45.4
0.06667	55.5
0.07078	60.5
0.07686	66.3
0.08438	75.6
0.08888	80.5
0.09658	85.6
0.13288	99.4
0.16593	110.8

Table A 6 Measured Friction Pressure Loss at 44°C

Measured Friction Pressure Loss (psi)	**Flow Rate (gpm)**
0.02918	30.4
0.03273	35.5
0.035	39.5
0.04542	50.5
0.05435	55.6
0.0714	64.5
0.07215	70
0.0896	83.4
0.105	91.5
0.12187	100.4
0.16347	114.1